Corrosion Science 242 (2025) 112551

Contents lists available at ScienceDirect

Corrosion Science

journal homepage: www.elsevier.com/locate/corsci

Characterisation of the deposition and protection performance of Zr conversion coatings on steel and zinc substrates using the response surface methodology

Ana Kraš [a,b], Davorin Kramar [c], Ingrid Milošev [a,b,*]

[a] Jožef Stefan Institute, Department of Physical and Organic Chemistry, Jamova c. 39, Ljubljana SI-1000, Slovenia
[b] Jožef Stefan International Postgraduate School, Jamova c. 39, Ljubljana SI-1000, Slovenia
[c] University of Ljubljana, Faculty of Mechanical Engineering, Laboratory for Quality Assurance, Aškerčeva 6, Ljubljana SI-1000, Slovenia

ARTICLE INFO

Keywords:
Low alloy steel
Zinc
EIS
Response surface methodology
Conversion coatings

ABSTRACT

The response surface methodology (RSM) was used to explore the experimental space, characterise the influence of deposition and drying conditions on corrosion resistance, and evaluate the interactions between these factors for zirconium conversion coatings on cold-rolled steel and zinc. A combination of non-electrochemical drop tests and electrochemical methods were utilised to evaluate corrosion resistance in a dilute Harrison's solution. The surface analysis confirmed the electrochemical results obtained under the conditions chosen by RSM. The uniform corrosion of both substrates guides the subsequent conversion process, while the best coating performance results from the interaction of pH, conversion time and bath concentration.

1. Introduction

Increasingly restrictive environmental and health legislation regarding chromate conversion coatings (CCCs) and phosphate conversion coatings has spurred interest in eco-friendly alternatives that can match or even surpass their performance [1,2]. Presently, only zirconium conversion coatings (ZrCCs) have matured for commercial applications. ZrCCs provide numerous advantages, including cost reduction (up to 30 %) due to faster conversion times, operation at room temperature, fewer process stages, smaller tanks, easier maintenance, and minimal sludge generation [3,4]. Conversion coatings, while fulfilling the role of primers to enhance the adhesion of subsequent layers, typically offer only a limited degree of corrosion protection. Yet, a corrosion failure in the conversion coating can quickly compromise the entire multi-coating system. Therefore, it is crucial to investigate conversion coatings for their corrosion resistance both individually and in conjunction with subsequent coatings. However, the existing scientific literature shows considerable variations in the results obtained from the same substrates and under similar conditions, ranging from poor performance to surpassing their predecessors [5].

Broadening the scope of ZrCC studies across diverse substrates is imperative, moving beyond the current focus on aluminium and its alloys and broadening it towards multi-metal applicability. Understanding the influence and possible interactions between ZrCCs and various bath conditions is crucial for achieving comparable or even superior performance to conventional conversion coatings. Consequently, this article emphasises a comprehensive investigation into two widely used substrates in the automotive industry [5–7]: cold-rolled steel (CRS) and pure zinc (as a substitute for galvanised surfaces herein [8,9]).[1] These substrates are investigated together due to observed similarities in the morphology of obtained ZrCCs, and the fact that they are more rarely represented in the literature compared to aluminium alloy substrates [5].

When several factors influence a particular process characteristic, the Design of Experiment (DoE), a family of statistical methodologies, could immensely help [10]. Using DoE, one can learn about the investigated process, differentiate between significant and insignificant factors, determine interactions between factors, construct predictive mathematical models, and optimise the response(s) [11]. Despite being widely adopted in industrial research after its inception over a century ago, the application of DoE in scientific research remains relatively limited. One of the primary merits of DoE lies in its ability to efficiently

* Correspondence to: Department of Physical and Organic Chemistry, Jožef Stefan Institute, Jamova 39, Ljubljana SI-1000, Slovenia.
E-mail address: ingrid.milosev@ijs.si (I. Milošev).

[1] Zn foil, being almost 100 % zinc, lacks intermetallic compounds such as δ and γ Fe-Zn found in typical galvanised steel, which improve corrosion resistance and durability. However, it was used herein as a simplified stand-in for galvannealed steel [8,9].

https://doi.org/10.1016/j.corsci.2024.112551
Received 7 August 2024; Received in revised form 2 November 2024; Accepted 3 November 2024
Available online 6 November 2024

explore the combined effects of several input factors in a smaller number of experiments. This starkly contrasts the traditional One Factor at a Time (OFAT) approach, which examines only one factor while keeping others constant, risking exploring only a partial experimental space and overlooking potential interactions between factors [10,12].

In DoE, when dealing with various influencing factors, the usual approach is to use a screening design to identify the most influential ones. However, one can also perform this initial screening based on experience and a thorough review of scientific literature and patents. We focused on investigating the conversion step using hexafluorozirconic acid (H_2ZrF_6) as a Zr-bearing component without incorporating common additives found in commercial ZrCC baths [13]. In addition, commercial cleaners, as per the manufacturer's recommendations, were utilised to comply with industrial applications.

Our assessment of pure H_2ZrF_6 conversion revealed that pH, concentration, and conversion time are the three most influential factors in the ZrCC process. Moreover, our experience suggests that the three factors contribute to the response independently and interact at specific levels [14–17]. From the industrial point of view, continued and replenished bath lines are desired, which could be achieved with lower concentrations and lower conversion times that will not leave the bath depleted, both of which are successfully resolved in ZrCC baths [18,19]. Following numerous commercial ZrCC bath recommendations, ZrCC baths typically operate at room temperature at H_2ZrF_6 concentrations from 150 to 1500 ppm, pH from 3 to 5, and conversion times from 60 to 900 s. This was addressed in our previous publication on the aqueous chemistry of Zr, especially regarding the distribution of Zr species as a function of pH [20]. The choice of this particular pH range was substantiated by the distribution of Zr aqueous species and the calculation of pH at which Zr(IV) hydroxide deposits [20]. Conversion time depends on the application method (shorter for spraying, longer for immersion) and the objective (adhesion improvement with shorter time, corrosion resistance with longer times/higher concentrations). Thicker coatings inherently provide enhanced corrosion protection; however, excessive primer thickness can accelerate the delamination of the topcoat [1,21]. However, both scientific and industrial literature lacks a consensus regarding the specific levels at which these factors should be used. Having three known influential factors with a wide range of values naturally leads to employing a response surface methodology (RSM) as a DoE method. RSM models relationships between multiple factors and the response of interest, identifying factor interactions and determining if the relationship is linear, quadratic, or more complex. What sets RSM apart from other experimental designs is its particular advantage of modelling quadratic effects, which is reflected as a curvature (non-linearity) in the relationship between input factors and the response [11,12]. To the best of our knowledge, very few studies have applied DoE in conversion coatings [22–28], and even fewer have utilised RSM [26–28]. Only one study has specifically applied RSM to investigate ZrCC. However, this study primarily focused on optimising ZrCC on a magnesium alloy before electrocoating [26].

Selecting an appropriate response for any experiment cannot be overstated. In this case, it is the corrosion protection of ZrCCs. However, the thin nature of ZrCCs, with thickness typically ranging between 10 and 50–80 nm [5], poses challenges in determining the optimal drying state, after which an evaluation is conducted. Further, using an excessively aggressive solution, like the commonly employed 3.5 wt% NaCl specified in well-established corrosion standards, such as ASTM G31–72 [29], can lead to excessive corrosion of less corrosion-resistant substrates, particularly noticeable when coated with thin films/coatings. Conversely, if the solution lacks sufficient aggressiveness, it may not effectively distinguish between samples with different corrosion susceptibilities [17,30–32]. In our opinion, using a dilute Harrison's solution (DHS) can be more convenient for assessing the aggressiveness of typical corrosion test electrolytes while still allowing for observing corrosion behaviour changes in thin coatings. DHS is a modification of the original Harrison's solution, presumably made by Timminis [33]. Using $(NH_4)_2SO_4$ together with a reduced amount of NaCl compared to a common 3.5 wt% solution has demonstrated more reliable results in predicting atmospheric corrosion. It has become a common choice for prohesion testing of primers [34–36] and has also been occasionally utilised, albeit rarely, in electrochemical testing of primers [37].

It is often neglected that electrochemical techniques are indeed complementary, and more should be employed simultaneously to describe the processes from different aspects [38]. However, such implementation is relatively infrequent in the existing literature. References such as [39,40] comprehensively tackled this problem. Among these techniques, destructive ones, such as potentiodynamic polarisation curves (PPC), directly examine the coating's integrity. However, they can alter or destroy the sample during testing, thus limiting sample variability and obscuring significant influences. On the other hand, non-destructive techniques such as electrochemical impedance spectroscopy (EIS) maintain the sample's integrity and offer higher sensitivity, enabling the detection of subtle variations and small differences between samples, thus exhibiting decreased reproducibility [41]. It would be highly advantageous to compare the credibility of these techniques in ranking the relative corrosion protection of different ZrCCs. In this study, several methods were integrated, and the results were critically assessed to choose the most relevant parameter from each method that represented the corrosion resistance of ZrCCs. Additionally, for comparison, we also employed an independent method for corrosion assessment, choosing a simple and convenient method known as the "drop test" [42]. Combining destructive and non-destructive techniques can provide a more comprehensive understanding of ZrCC's behaviour, performance, and potential degradation mechanisms [35,42–44]. In fact, our preliminary RSM study encountered numerous problems related to properly evaluating such thin coatings, which is not a straightforward task and is often misinterpreted in the literature. By expanding the experimental scope through RSM to address data reliability issues in thin film analysis and enhance result credibility, we believe we can offer valuable insights into ZrCC. This is based on our previous basic research studies [20,45] and sets the groundwork for future research on various substrates and additives.

2. Experimental

2.1. Materials

Low-carbon cold-rolled steel (CRS) was used as a 1 mm thick panel (ACT Test Panels LLC, Hillsdale, Michigan, USA) with the chemical composition obtained by X-ray fluorescence spectroscopy: C 0.04 wt%, Mn 0.2 wt%, S 0.01 wt%, Fe remainder. Zinc was supplied as a 1 mm thick foil (Goodfellow Cambridge Ltd., UK) with a manufacturer-specified chemical composition: 98.8 % Zn.

Original panels were cut into smaller 2.5 cm × 3.5 cm square sheet specimens with 3 mm diameter holes punched for easier immersion into H_2ZrF_6 conversion baths. For surface analysis, samples were cut out to dimensions of up to 1 cm^2.

2.2. Chemicals

Solutions used in this work were prepared from as-received analytical reagent grade chemicals: absolute ethanol (EtOH, Merck KGaA, Darmstadt, Germany), NaCl (Fisher Scientific, Leicestershire, UK), $(NH_4)_2SO_4$ (Acros Organics Geel, Belgium), NH_4HCO_3 (Sigma-Aldrich, Steinheim, Germany), H_2ZrF_6 (50 wt% in water, Sigma-Aldrich, Saint Louis, USA), $CuSO_4 \times 5\,H_2O$ (Sigma-Aldrich, Saint Louis, USA), HCl (37 %, VWR International S.A.S, Fontenay-sous-Bois, France) Pb $(CH_3COO)_2 \times 3\,H_2O$ (Sigma-Aldrich, Saint Louis, USA). For chemical pretreatments, SurTec®'s chemical products (SurTec International GmbH, Bensheim, Germany), supplied by SurTec Adria, d.o.o. (Ljubljana, Slovenia) were used: SurTec® 089, SurTec® 132 and SurTec® 141. SurTec® 089 is a detergent booster concentrated liquid product

containing non-ionic surfactant alcohols in ethoxylated forms of amines, alkyls and fatty alcohols. SurTec® 132 is a slightly alkaline builder, free of silicates and surfactants, containing tetrapotassium pyrophosphate. SurTec® 141 is an alkaline builder, free of surfactants, containing phosphates, sodium tetraborate and silicates.

Milli-Q Direct water (Millipore, Billerica, Massachusetts, USA) with a resistivity of 18.2 MΩ cm at 25 °C and the total organic carbon (TOC) value below 5 ppb was used for rinsing samples and solution preparation.

2.3. Samples and solutions preparation

2.3.1. Grinding

The first step in sample preparation was manual wet-grinding with SiC papers up to P4000 grit on a LaboPol-5 grinding/polishing machine at 300 rpm (Struers, Ballerup, Denmark). Grinding to a P4000 grit was considered sufficient to ensure appropriate roughness ($R_a \approx 20–30$ nm) for applying nanometric ZrCC coatings. After grinding, samples were cleaned by 5-minute ultrasonication in absolute ethanol using a 37 kHz, 100 % power Elmasonic P ultrasonic bath. Finally, samples were rinsed with absolute ethanol and Milli-Q water and dried with compressed N_2.

2.3.2. Chemical pretreatment

The aim of the chemical pretreatment step was, besides impurity removal, to ensure a hydrophilic surface for successful zirconium conversion [46]. A simple "water-break test ", when rinse water evenly coated the entire sample surface after cleaning, was used to indicate efficient surface cleaning [21,47]. Chemical pretreatment before conversion was performed via alkaline cleaning by immersion in respected SurTec® solutions on a C-MAG HS 7 magnetic hotplate stirrer (IKA®--Werke GmbH & Co. KG, Staufen, Germany) under stirring rate of 150 rpm and temperature of 60 °C, according to lab-modified SurTec's recommendations for each substrate.

For CRS: a 5 min alkaline cleaning in 5 vol% (50 mL/L) SurTec® 132 + 0.6 vol% (6 mL/L) SurTec® 089, pH=7.3

For Zn: a 5 min alkaline cleaning in a mixture of 2 vol% (20 mL/L) SurTec® 141 + 0.5 vol% (5 mL/L) SurTec® 089, pH=12.8

As typical for non-aluminium substrates, no acidic desmutting step was used after alkaline cleaning. Each alkaline cleaning step was followed by a double rinse with Milli-Q Direct water: (i) ca. 30 s rigorous circular rinse with a wash bottle on both sample sides, and (ii) a 1-minute dip in a clean Milli-Q Direct water bath. Glass beakers (V = 500 mL) were used for rinsing baths. Since ZrCCs are extremely sensitive to alkaline contamination, at least two rinses are required between the cleaner and coating stages [48].

2.3.3. Conversion treatment

Immediately after the chemical pretreatment, samples (with the entire surface still wet) were immersed in H_2ZrF_6 conversion baths with different combinations of factor settings predetermined by the chosen RSM design, as described in the following section.

Since zirconia precipitation from H_2ZrF_6 occurs at a relatively low pH (3−5) [5,20], H_2ZrF_6 solutions were prepared by diluting 50 wt% H_2ZrF_6 solution firstly in a small volume of water and filled up to the final volume, while the pH was set under vigorous stirring using a diluted (15 wt%) NH_4HCO_3 solution that also serves as a buffer, prolonging the lifetime of prepared baths [21]. pH was measured using an 827 pH-lab pH meter connected to a Solitrode HF combined pH electrode suitable for measurements in HF and F-containing solutions (Metrohm AG, Herisau, Switzerland).

Teflon beakers (V = 250 mL) were used for conversion baths. Samples were immersed in conversion baths and hung onto a plastic stick. Prepared H_2ZrF_6 solutions were stored in polyethylene bottles due to HF release with pH increase [20].

The conversion bath was not stirred, as it was preliminarily observed that stirring with our set-up leads to less uniform coating formation (not shown). Consequently, samples were occasionally lightly moved back and forth through the conversion bath to allow fresh solution access to the surface, a practice occasionally observed in industrial settings with manual immersion.

After conversion, the samples were rinsed again using two steps: (i) a vigorous circular rinse with a wash bottle on both sides of the sample for approximately 30 seconds, and (ii) a 1-minute dip in a clean Milli-Q Direct water bath. In addition to removing unreacted chemicals and residues from the bath before drying, this process also aids in reducing fluoride through ion exchange between F^- and OH^-, as anions are consistently retained in zirconia during precipitation at pH levels below 7 [49–51]. Finally, the samples were dried using a stream of compressed N_2 in the bottom-up direction and dried for 10 min at 80 °C on a C-MAG HP 4 hotplate (IKA®-Werke GmbH & Co. KG, Staufen, Germany), according to common industrial practice. One series of samples for drop tests and electrochemical measurements on Zn were performed after leaving them to air-dry to assess the influence of drying.

2.4. Response surface methodology

After an extensive review of the available literature, a range of H_2ZrF_6 concentrations from 150 to 1500 ppm, pH levels from 3 to 5, and conversion times from 60 to 900 s were explored. RSM results, along with all additional information such as ANOVA (analysis of variance) test results, model adjustments for each RSM response across both substrates and a concise theoretical background on DoE and RSM, are provided in the Supplementary material, Sections 1 and 3. These factor-setting combinations are somewhat counterintuitive from the traditional point of view of planning the experiments, yet these make design models with high predictive power, enabling process insights from fewer measurements.

Investigating such a range using a central composite design (CCD) of RSM (Fig. 1b) resulted in the variation of all factors at 5 levels: concentration was varied at 150, 424, 825, 1226 and 1500 ppm, pH was varied at 3.0, 3.4, 4.0, 4.6 and 5.0 and conversion time was varied at 60, 230, 480, 730 and 900 s, as presented in Table 1. It must be noted that such a wide parameter range, spanning an order of magnitude, is commonly employed in screening experiments. This approach is initially used to identify the most influential factors, followed by a more detailed design to understand better and characterise the process. However, it is important to consider that if the model successfully explains variability within the chosen parameter range—validated through statistical analysis, regression models, and assessments of goodness of fit—it confirms the suitability of the selected range. Only the centre point (825 ppm/480 s/pH 4.0) was sextuplicated, according to the postulation of RSM.

Corrosion resistances obtained by different non-electrochemical and electrochemical methods were chosen as RSM responses for cold-rolled steel and zinc substrates to compare their sensitivity and feasibility for observing the effects of conversion bath parameters. For an easier follow-through, the sample preparation, measurements and important factors considered are given in the form of a flowchart in Fig. 1a.

2.5. Measurements of corrosion resistance

2.5.1. Non-electrochemical measurements

First, a straightforward and non-electrochemical approach known as the drop test was used, indicated by a change in colour, signifying that the reagent cations reached the bare metal surface, enabling their reduction (Cu or Pb herein). For CRS, "Akimov's reagent" [42] was used (82 g/L $CuSO_4 \cdot 5\,H_2O$, 33 g/L NaCl, and 13 mL/L of 0.1 N HCl, pH=3.6), while $Pb(CH_3COO)_2$ (50 g/L, pH=5.6) was used for Zn as it was preliminarily shown that the use of Akimov's reagent was too aggressive, leading to the instant dissolution of Zn-ZrCC samples, presumably due to an excessively acidic pH for Zn. The time required for colour to change after dropping the reagent on top of the non-coated and coated substrates was measured using a stopwatch and is called the "protective

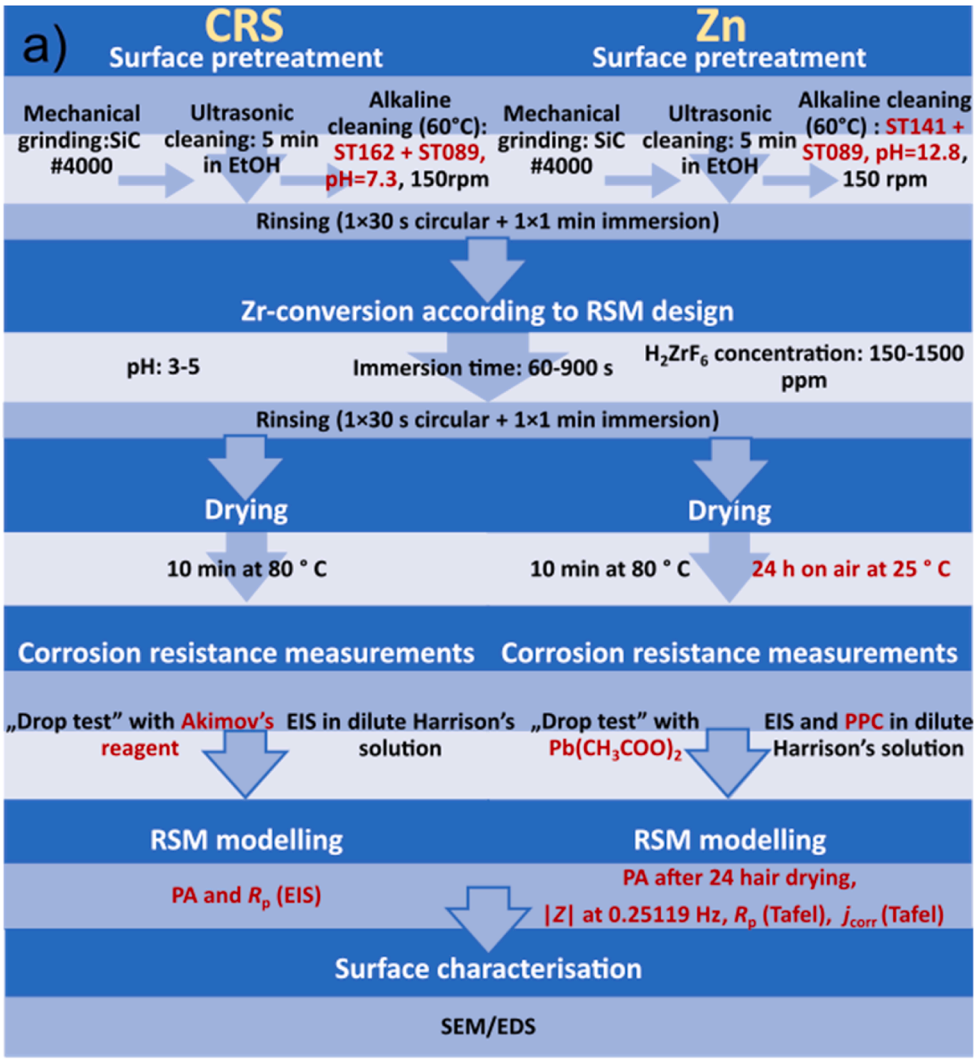

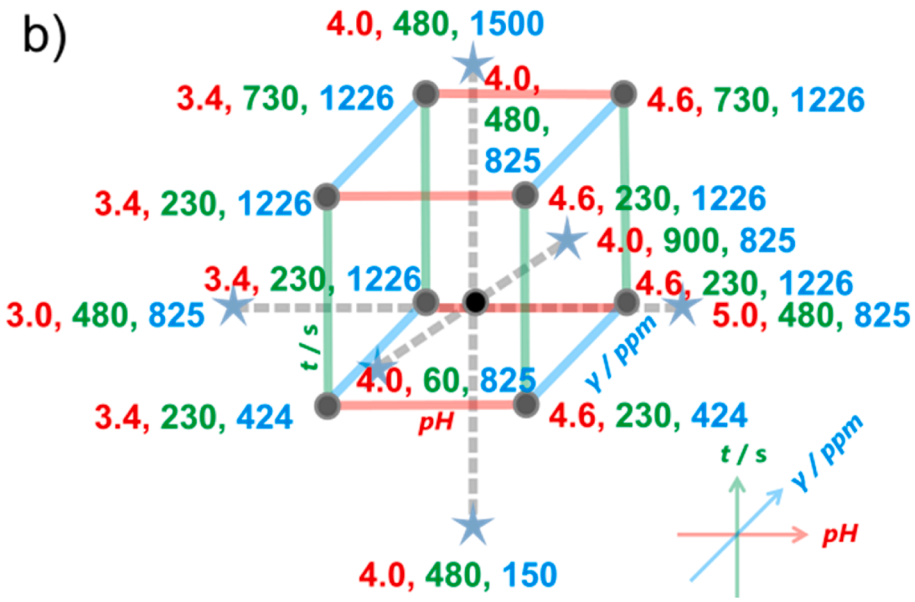

Fig. 1. (a) Schematic summary of sample preparation, RSM design, electrochemical measurements, RSM modelling and SEM/EDS characterisation. The differences between the sample treatments are highlighted in red. (b) The CCD design employed for substrates.

Table 1
Summary of central composite design (CCD).

Factor	Name	Units	Type	SubType	Minimum	Maximum	Coded Low	Coded High	Mean	Std. Dev.
A	pH		Numeric	Continuous	3.00	5.00	−1 ↔ 4.00	+1 ↔ 4.59	4.08	0.4582
B	*t*	s	Numeric	Continuous	60.00	900.00	−1 ↔ 230.27	+1 ↔ 480.00	439.03	194.78
C	*c*	ppm	Numeric	Continuous	150.00	1500.00	−1 ↔ 150.00	+1 ↔ 825.00	693.16	377.00

ability" (PA); the longer the time for colour change (to red for CRS and black for Zn), the better the PA. A representative example is given in the video in the Supplementary material. PA measurements were conducted following conversion with a 10-minute drying period at 80 °C for both substrates and, additionally, after 24 h for Zn.

2.5.2. Electrochemical measurements

Electrochemical experiments were carried out with a Multi Autolab/M204 (Metrohm Autolab, Utrecht, Netherlands) potentiostat/galvanostat controlled by Nova 2.1. software. Measurements were conducted in homemade modified "clamp-on "electrochemical cells (250 mL), which are suitable for flat, thin-coated samples and less susceptible to crevice corrosion [30]. Respective cell parts were custom-made and assembled by bonding with a strong 1-component solvent adhesive ACRIFIX® 1S 0116 (Evonik Performance Materials GmbH, Darmstadt, Germany). Electrochemical measurements were performed in a three-compartment set-up: the sample as a working electrode (WE) was attached to the bottom by pressing it against an o-ring, which allowed for the easier escape of gas bubbles formed by cathodic reactions, presumably reducing the risk of crevice corrosion. A carbon rod was used as the counter electrode (CE), and a saturated Ag/AgCl (3 M) electrode was used as the reference electrode (RE); $E = 0.297$ V vs. standard hydrogen electrode, set near the WE, to minimize the uncompensated IR drop. All potentials herein are referred to the Ag/AgCl (3 M) scale. The area of the working electrode was 0.785 cm^2. All measurements were performed at ambient conditions.

Before electrochemical measurements, samples were allowed to rest at the open circuit potential (OCP) and monitored for a conditional time until reaching a quasi-stable state. The rest period was followed by measurements of electrochemical impedance spectra (EIS) and potentiodynamic polarisation curves (PPC). This decision was made because there was no risk of electrode alteration due to an excessively high chosen amplitude used in EIS in this particular case. The additional experimental improvement would include separate measurements of cathodic and anodic polarisation curves due to possible changes during the cathodic scan. Due to many experiments, however, the anodic and cathodic branches of PPCs were not measured separately.

To lower the effect of electrolyte aggressiveness inducing corrosion already at the rest potential, the time for OCP measurement was modified for each substrate: samples of CRS, as they started to corrode already at OCP, were left to approach Kelly's recommendation of stationary-state approximation when 5 mV does not change over a 10 min period, which was in most cases established in 20–30 min [52]. Zn samples that indicated metastable pitting during OCP were arbitrarily left to stabilize for 300 s.

EIS spectra were recorded at the OCP with a perturbation potential amplitude of ± 10 mV (root mean square). A range of 51 logarithmically spaced frequencies were applied across 7 decades, from 100 kHz to 10 mHz. The EIS data was fitted using the NOVA 2.1 software, which employs a nonlinear least-squares regression approach to fit the experimental data to the equivalent circuit model using the Levenberg-Marquardt optimisation algorithm. The iR drop compensation was not considered, as all samples exhibited an iR drop of less than 1 mV at low frequencies.

Potentiodynamic polarisation curve measurements were conducted in the potential region starting from −150 mV vs. OCP to 1 V vs. reference electrode in the anodic direction until the current reached 1 mA or 1 V. The scan rate was 1 mV s^{-1}. Tafel extrapolation method to extract corrosion parameters (corrosion potential, E_{corr}, and corrosion current density, j_{corr}) from PPCs was performed using Nova 2.1 software, from which polarisation resistance (R_p) was calculated according to the standard ASTM G59–97 [53].

The electrolyte in the study was a dilute Harrison's solution (3.5 g/L $(NH_4)_2SO_4$ and 0.5 g/L NaCl, pH = 5.2) usually used for the simulation of atmospheric conditions and a trade-off between corrosivity of the solution and ability to rank corrosion properties between different ZrCCs.

Corrosion resistances assessed by different electrochemical parameters were used in RSM (Table 2). For CRS, R_p was determined only from EIS. In the case of Zn, the impedance modulus ($|Z|$) measured with EIS at a frequency of 0.25119 Hz was used along with R_p from PPC (*vide infra*). In addition, for Zn, the j_{corr} was derived from PPCs. Thus, the criteria for selecting the best H_2ZrF_6-based ZrCC bath conditions were founded on the maximal R_p and minimal j_{corr}.

2.5.2.1. EIS experimental details. Making an unambiguous assignment of certain time constants is facilitated by performing EIS measurements under various conditions. These conditions exert different influences on specific time constants, for example, by altering the electrolyte properties (pH, concentration) [54], utilising time-resolved measurements, modifying the perturbation potential, or repeating measurements at specific perturbation potentials [55,56]. Additionally, advanced surface analysis techniques are desired to study the exact layer structure. Rather than that, in this work, the power of analysing EIS spectra obtained from a larger set of samples is leveraged to unravel the different time constants. In addition, the selection of equivalent electrical circuits (EECs) was based on prior knowledge of both the substrate and ZrCC behaviour in NaCl-containing solutions, comparing the presence/absence of specific time constants compared to the bare substrates.

After EIS measurements, samples were checked to comply with EIS conditions for stability, causality and linearity by analysing raw AC potential and current data, either through the Kramer-Kroning's test, Lissajous and AC current / AC potential resolution plot [56] (not shown). Raw EIS data analysis tools are readily available and, as such, were used in NOVA software.

Following Occam's razor principle [56], the proposed EECs for fitting EIS spectra consist of the minimum number of elements required for the physical interpretation of the data. Emphasis was given to obtaining the best predicting and not fitting model that captures major electrochemical processes. Therefore, the proposed models are only tentative but have proved helpful in interpreting the effects of conversion bath parameters. The number of time constants relied solely on visual inspection of Nyquist and Bode plots, i.e., symmetry in phase angle peaks and capacitive arcs and the analysis of fit residual errors. Periodicity in residual error analysis indicated that not all-time constants have been considered [57]. Connections of Voigt elements incorporating CPE were used to describe different electrochemical phenomena. CPE instead of C was employed to compensate for the distribution of relaxation times caused by surface inhomogeneities [58]. In all cases involving multiple time constants, a "ladder" R-CPE circuit [58] was utilized ([R([R(RCPE)]CPE)], further justified by the developed porosity in the obtained ZrCC and substrate oxide film, where both the substrate and coating are exposed to the electrolyte. In the case of a ladder circuit, a resistance is connected in series to a parallel combination of another RCPE couple. A ladder circuit instead of a serial connection of Voigt elements also resulted in lower fit residual errors

Table 2
Comparison of the feasibility of each technique (Protective ability (PA), potentiodynamic polarization curves (PPC) and electrochemical impedance spectroscopy (EIS)) and responses for evaluating ZrCCs on CRS and Zn.

Technique		Protective ability		PPC		EIS
Substrate: CRS	**Response**	PA after drying at 80 °C		j_{corr}	R_p	R_p
	Applicable to RSM	no		no	no	**yes**
Substrate: Zn	**Response**	PA after drying at 80 °C	PA after air-drying for 24 h	j_{corr}	R_p	$\|Z\|$ at 0.25119 Hz
	Applicable to RSM	no	**yes**	no	sufficiently reliable	**yes**

(not shown).

Unfortunately, as a reference shunt has not been used herein [59,60], the high-frequency inductance (above 10^5 Hz) was affected by the RE impedance, making it difficult to determine small capacitive loop impedances at high frequencies accurately. However, this influence was limited to the high-frequency region and did not affect the mid- and low-frequency regions, which are of greater interest for coating evaluation.

If diffusion or induction effects were observed at low frequencies but within a narrow range, they were disregarded since they did not dominate corrosion behaviour. Instead, the effects that exhibited a more capacitive behaviour, as determined by the fitted value of *n*, were used for coating evaluation.

2.6. Surface analysis

After grinding up to 4000 grit, samples for SEM imaging were further polished using a 1 μM diamond suspension Dia-Duo 2 on an MD-Nap polishing cloth (Struers, Ballerup, Denmark). Cleaning and conversion steps were performed in Petrii dishes in non-stirred solutions due to the smaller sample size than those used for non-electrochemical and electrochemical measurements. In addition, Zn samples for SEM were allowed to air-dry for 24 hours.

SEM analyses were performed using a field emission SEM JSM 7600 F, JEOL, Japan, equipped with energy dispersive X-ray spectroscopy (EDS) (Inca Oxford 350 EDS SDD). SEM images were recorded in secondary electron (SE) and back-scattered modes using a concentric backscatter (CBS) detector. A beam voltage of 5 kV was used. Before analysis, samples were coated with a thin carbon layer to reduce the charging effect.

3. Results and discussion

After selecting the CCD design for the experiments (Table 1, Fig. 1b), the non-electrochemical and electrochemical measurements were conducted and analysed. As will be described below (Table 2), some results were not used for further procedures in RSM since they were evaluated as scientifically unreliable. The other results were confirmed as scientifically sound to represent differences between coated and non-coated samples and were used for RSM analysis.

3.1. Non-electrochemical results

A drop test was used as a fast screening method employing the change in colour as a parameter of protective ability (PA). It is important to note that, in our case, determining the exact endpoint of the complete colour change with this method was somewhat subjective. The duration often varied by a few seconds and could be influenced by splashes from hydrogen evolution reaction (HER) under certain conditions. Nevertheless, this does not diminish the method's usefulness for detecting changes when the time difference is above 10 seconds. For CRS, the drop test was conducted after 10 min drying at 80 °C using a so-called Akimov reagent. When comparing all CRS-ZrCC samples to the ZrCC-free ones, it is observed that the bare sample demonstrates the highest PA (19 s) (Table S5). In contrast, the PA was 11 s for the alkaline cleaned sample. However, the noteworthy resistance of the bare sample can be attributed to its hydrophobic nature (deduced only visually by the water droplet shape), which is significantly diminished following alkaline cleaning, subsequently facilitating the deposition of ZrCC (Table S5). Consequently, the alkaline-cleaned sample shows values comparable to those of ZrCC-treated samples due to higher hydrophilicity in both cases, presumably undesirable for corrosion resistance. However, this property is counterbalanced in ZrCCs to enhance the adhesion of subsequent organic coatings. Despite the alkaline cleaned sample showing values comparable to those of ZrCC-treated samples (between 6 and 13 s), it is important to note that the observed colour variations in the formed coatings on CRS (ranging from gold to purple with an increase in conversion time, indicating increased thickness) and the resulting hue of red during copper reduction hint at the existence of certain corrosion protection benefits offered by ZrCC-treated samples. This becomes especially apparent when later considering cases where the drop colour's hue appeared more pink than red on well-performing ZrCC samples, in contrast to the reddish hue observed in poorly performing and ZrCC-free samples. However, both the ZrCC colour and the drop colour were not chosen as RSM responses because they involve categorical factors necessitating a higher number of descriptors, which, unfortunately, remains unaddressed here, given the limited range of possibilities (pink or red, purple or gold).

For the Zn substrate, the drop test was conducted after 10 min drying at 80 °C and 24-h air drying using Pb(II) acetate and HCl. The colour changed to black once the substrate was reached. After 10 min drying at 80 °C, Zr-free substrates had PA of 0 s, whereas ZrCC-coated between 9 and 25 s (Table S6). After 24-h air drying, Zr-free substrates exhibited PA of 11 s and 12 s, and ZrCC-coated between 9 and 25 s. All the PA values were then used as input parameters for RSM.

Some samples that initially seemed to exhibit better corrosion protection failed after 24 hours (Table S6), emphasising the importance of assessing the conversion coating as a mixture of ZrCC and native oxide, as implicated in [14,61] and another confirmation of the hypothesis of taking into account the Pilling-Bedworth ratio when considering native oxide growth inside thin films on different substrates.[2] However, while appearing essential to boost the primer's corrosion resistance, it is noteworthy that the resulting oxide film might exhibit distinct adhesion properties from the primer [62].

3.2. Electrochemical results

The main text contains only discussion-relevant electrochemical results for ZrCC-coated substrates prepared based on the parameters set by RSM (Table 1, Fig. 1a). All the other results are given in the Supplementary material, Section 2.

[2] For successful conversion coating, the oxide layer must dissolve, exposing the fresh substrate to the bath. The difference between 10 minutes and 24 hours of drying suggests film reinforcement, likely due to the substrate's native oxide growth during air exposure, with corrosion resistance approaching that of ZrCC-free samples. Ongoing ellipsometric studies aim to confirm changes in the oxide film on the substrate or the zirconia coating, though we believe the latter is minimally affected by one day of dehydration, as its growth is limited, unlike the substrate oxide, which can continue to expand. This is further reinformed that the corrosion resistance of ZrCC on CRS does not improve with prolonged air exposure.

3.2.1. Potentiodynamic polarisation curves

3.2.1.1. Cold-rolled steel. PPCs measured in dilute Harrison's solution for CRS on one of the best- (825 ppm/480 s/pH 4.0) and one of the least-performing ZrCC-coated samples (424 ppm/230 s/pH 3.4) along with ZrCC-free samples are depicted in Fig. 2a and Table S1. PPC curves for ZrCC-free samples are similar, with a slight improvement in the alkaline-cleaned sample. Among the ZrCC-coated samples, which show only slightly decreased j_{corr} values compared to ZrCC-free ones, another distinction lies in a slight anodic shift and inconclusive differences in current density values compared to bare samples; intriguingly, the sample with poorer performance displays almost the same and slightly improved current density values compared to the supposedly better one. Assuming porosity formation in CRS-ZrCC during electrolyte exposure (*vide infra*), these pores might serve as anodic sites, potentially leading to ZrCCs displaying worse PPC results than ZrCC-free samples, as shown in [63]. Essentially, the tiniest defect within such a thin coating suffices to trigger corrosion during the anodic potentiodynamic scan. This is further demonstrated by the fact that there was no significant difference between the two represented ZrCC samples in PPC curves, justifying the decision to forego further PPC analysis on CRS samples.

3.2.1.2. Zinc. Concerning Zn (Fig. 2b-d), Table S2, PPCs reveal no consistent alterations in corrosion potential or passivation region. PPC results in DHS for ZrCC-free samples and ZrCC-coated CRS samples are depicted in Fig. 2b together with the best- and least-performing samples, repetitions of the central point (Fig. 2c) and the remaining results presented in Fig. 2d. However, there is a marginal reduction in corrosion current densities compared to ZrCC-free samples, although within a similar order of magnitude. As a result, further confirmation through ANOVA is necessary to ascertain statistically significant differences (Supplementary material, Section 3), as will be explained below. A clearer presentation of the PPC curves separated into additional graphs for better distinction compared to Fig. 2b-d can be found in the Supplementary material, Figure S1.

The decision to restrict PPC response in RSM methodology *(vide infra)* solely to Zn substrates while excluding CRS samples (Table 2) was based on observations of a general improvement of ZrCC treatment on Zn, as opposed to an anodic shift in E_{corr} values and significant corrosion resulting from the destructive nature of PPC on CRS.

3.2.2. Electrochemical impedance spectroscopy data

3.2.2.1. Cold-rolled steel. EIS results in DHS for Zr-free samples and ZrCC-coated CRS samples are depicted in Fig. 3 and divided into three graphs: (a) selected samples chosen for discussion, (b) repetitions of a central point and (c) remaining results not presented in (a). ZrCC-coated samples exhibited either one (EEC in Fig. 3d) or three-time constants (EEC in Fig. 3e), which directly correlate with the amount of ZrCC coating present and the formation of iron corrosion products, as will be described below. By theory, the first time constant is ascribed to the coating, while the second is to the corrosion process [55]. However, the assumed developed porosity in ZrCC along with iron corrosion products, implies that EIS spectra can show features related to both geometric and kinetic phenomena [64].

The first unresolved high-frequency time constant (insets of Fig. 3a-c) with a small capacitive loop (up to 100 Ω, which was not fitted as its value is negligible and due to high-frequency (HF) effects induced by reference electrode) can be ascribed either to electrolyte resistance inside pores at the passive film/electrolyte interface, with an interfacial capacitance of the pore wall or to the dielectric properties of the barrier surface film [58]. Thus, the EEC, including only two time constants, was used for cases displaying three time constants, as shown in Fig. 3e, by excluding the component R_{HF}-CPE_{HF} from fitting. This is another confirmation of the inadequacy of using PPC for ZrCCs corrosion evaluation on CRS. Most probably, interconnected pores developed in the coating during exposure to electrolyte result in the shape of the obtained PPC being similar to that of the bare substrate [65].

The second, middle-frequency time constant (R2-CPE1) can be ascribed to the charge transfer resistance (R_{ct}) of faradaic reactions inside defects and CPE1 to a double layer capacitance, i.e., the capacitance at which those reactions occur [66]. On the other hand, the third time constant in the low-frequency range (R3-CPE2), although not fully resolved due to limited low-frequency (LF) measurements, can be linked, based on n values, to capacitive behaviour associated with the capacitive response of corrosion products. The R3 value at LF can be attributed to the relaxation of the corrosion products on the electrode surface [66–71]. Further confirmation was provided after a 24-hour immersion in DHS, which resulted in a change in only the third time constant. This change was observed as an increase in capacitance and a decrease in R3, attributable to rust layer growth. Notably, no alterations were observed in the other time constants, indicating that the ZrCC remained intact and that the developed rust layer was non-protective, not affecting the charge transfer resistance, as shown in Fig. S2 in the Supplementary material, Section 2.

FTIR analysis also revealed the formation of lepidocrocite (γ-FeOOH) during exposure to DHS, as indicated in Fig. S3 in the Supplementary material, Section 2, aligned with previous reports of lepidocrocite formation in low-aggressive corrosion environments [72]. The Pilling--Bedworth ratio indicates the development of non-protective oxides for iron (and its alloys) due to the larger volume of the oxide compared to its metal elementary cell, leading to rupture and enabling further corrosion through the rust layer [73]. Taking into account all these results and the fact that lepidocrocite exhibits high porosity, a layer of rust can be assumed to grow on top of ZrCC [67,72].

Nevertheless, all CRS-ZrCC samples that exhibited three time constants show improvement in R_{ct} (R2) values, owing to ZrCC (Supplementary material, 1, Table S3). On the other hand, the sample prepared at 825 ppm, 60 s and pH 4.0 and samples prepared at pH < 4.0, except for those prepared at longer conversion time (730 s), all show only one time constant, comparable to ZrCC-free samples, as a result of a merge of other time constants into a single R-value, probably dominated by R_{ct}, indicated that no ZrCC coating has formed. In addition, all samples treated at pH ≥ 4.0 and 730 s exhibited smaller values of R3, likely due to increased porosity caused by higher thickness (Table S3). Nevertheless, due to the overlap of time constants and the thin nature of formed films, for the overall evaluation of the CRS-ZrCC system with RSM, the polarisation resistance, R_p, expressed as the sum of the main two resistances obtained by EIS [74] was used as an input parameter for RSM. Although sharing the same order of magnitude, R_{ct} can be approximated by R_p measurements from DC methods [74] such as LPR (linear polarisation resistance) [75] or PPC; however, due to the inherent capability of EIS to capture multiple processes and non-destructiveness, the latter is preferred, as will be shown by RSM results.

3.2.2.2. Zinc. Zn samples exhibited a very small unresolved high-frequency time constant that can be attributed either to a barrier layer of ZnO (arising from alkaline cleaning or etching with H_2ZrF_6) (Fig. 4a-c, Table S4) or porosity effects, the latter being more probable, as most samples exhibited a more or less prominent, distorted, high-frequency tail typical for porous electrodes [76,77]. However, all Zn samples exhibited significant diffusional effects, as shown by a large second time constant in low concentrations and short conversion times, and distorted semicircles in the rest of the cases with n values between 0.1−0.3. This is similar to cases in [78–80]. Diffusion effects probably arise from the diffusion of species from the bulk or formation of corrosion products. Thus, the width of capacitive arcs in Nyquist spectra can be referred to as diffusion resistance.

In the latter case, Lissajous plots and Kramer-Kronig tests indicated

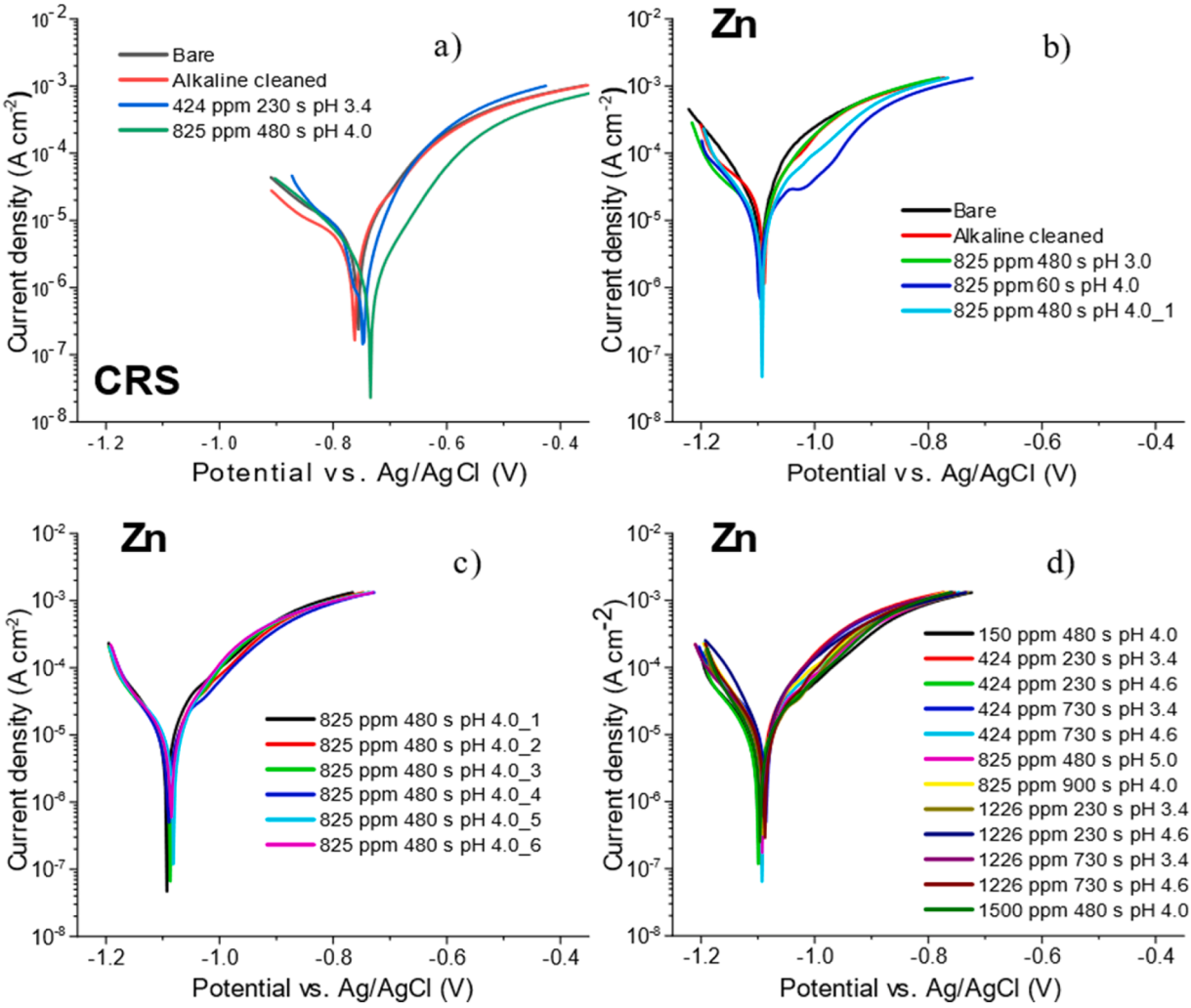

Fig. 2. Potentiodynamic polarization curves in dilute Harrison's solution recorded for (a) CRS and (b-d) Zn. (a) selected best- and least-performing ZrCCs on CRS, (b) chosen Zn-ZrCC results for discussion, c) Zn-ZrCC results of central point repetitions, d) Zn-ZrCC results obtained under the remaining conditions. dE/dt = 1 mV/s. Bare and alkaline-cleaned substrates are presented in (a) and (b). Rest periods at OCP were (a) 20−30 min, and (b-d) 300 s. A clearer presentation of the PPC curves, separated into additional graphs for better distinction compared to Fig. 2b-d, can be found in the Supplementary material, Fig. S1.

that these fluctuations signify instability during measurements. This instability is likely due to inconsistent conversion layer formation, resulting in the accumulation of corrosion products and their related diffusion [72]. Therefore, fitting was not conducted. Instead, an absolute impedance value at a chosen frequency of 0.25119 Hz was employed as a corrosion resistance response. This decision was based on the most significant deviation between high and low diffusion resistances observed at that frequency. Moreover, this frequency aligns with the conclusion of the middle time constant when visual distinction is feasible – likely indicating charge transfer resistance. Afterwards, it was observed that this very frequency also confers more weight to well-performing samples in drop tests and less weight to poorly performing ones. Hence, it can serve as a convenient corrosion evaluation parameter for ZrCCs on Zn, effectively accommodating RSM results and providing a more comprehensive grasp of ZrCC process behaviour.

However, it is important to note that the samples displaying high diffusion resistance during EIS measurements also displayed stability during measurement and passed Lissajous and Kramers-Kroning test analysis. These samples were indeed eligible for fitting (EEC from Fig. 3e), indicating a finite length transmissive boundary case modelled by an O-element (open boundary finite length diffusion) [58]. In this case, a fixed diffusion layer with a fixed thickness can be considered as being contained in the solid film, both ZrCC and corrosion products.

However, it has been observed that the O-element cannot efficiently model that behaviour, as n values of CPE are very close but not exactly 0.5 when employing a Voigt element to fit the diffusion constant, suggesting deviation from typical diffusion behaviour.

Using an RCPE element to represent diffusional effects is justified because putting a resistor in parallel to capacitance always describes a process involving energy dissipation (resistor) co-occurring with energy storage (capacitor) [56,58]. As a matter of fact, it has been shown that using RCPE can be more accurate in describing an O-element [81–84] and has already been employed in conversion coating studies [66,85]. In that case, R accounts for diffusion resistance, i.e., growth of the diffusion layer, while accompanying admittance of CPE represents diffusion of charge carriers. The increase in diffusion resistance can be attributed to the thickening of the diffusion path, possibly due to forming a more compact corrosion product layer. On the other hand, the increase in admittance values is associated with forming a less dense film, whether it is the ZrCC or Zn corrosion products layer, similar to the EIS investigation on CCCs on Alclad 2024-T3 by Campestrini et al. [66]. This would also explain that the corrosion process has reached a steady state due to reduced corrosion resistance on samples with lower ZrCC thickness. Finally, in the case of the Zr-free, bare Zn sample (Fig. 4a), a very high diffusion resistance value is observed, reaching infinity and resembling the behaviour of a pure W-element [56,58], which is most likely a result

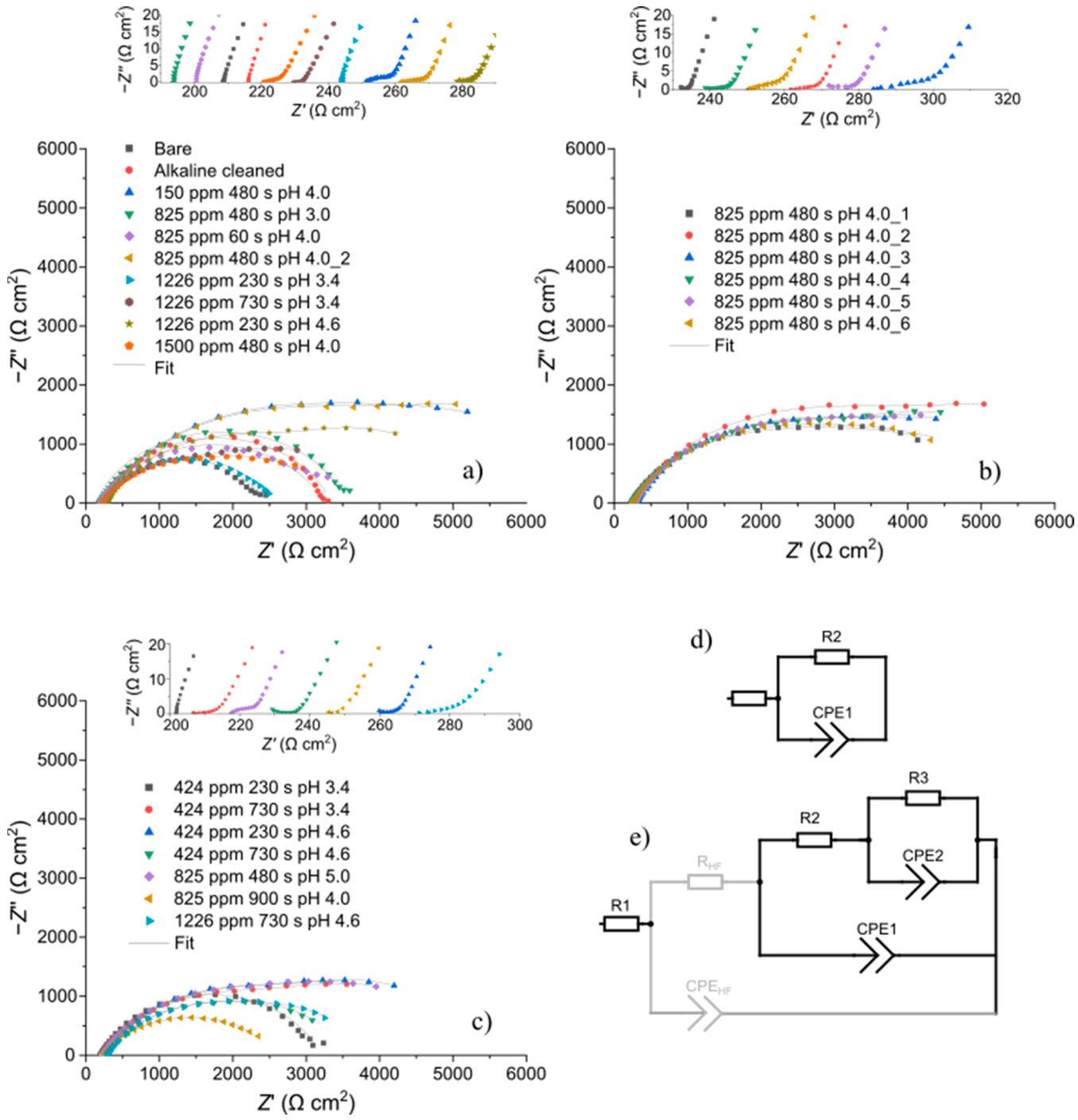

Fig. 3. EIS results for CRS-ZrCC in dilute Harrison's solution with insets at high frequencies: (a) chosen results for discussion, (b) results of central point repetitions, (c) results obtained under the remaining conditions. Bare and alkaline-cleaned substrates are presented in (a). EECs used for EIS fitting: (d) Bare CRS, CRS-ZrCC treated at pH < 4.0, with conversion time > 60 s, (e) CRC-ZrCC samples treated at pH ≥ 4.0 and conversion time ≥ 230 s. Please note that R_{HF} and CPE_{HF} components were not used for fitting. Rest periods at OCP were 20 min.

of the growth of a thick and porous Zn corrosion products layer, as will be shown in the text below by SEM analysis.

It is noteworthy that any deviation from perfect, semi-infinite linear behaviour should result in disturbance of the diffusion process, most likely by more influences at the same time. "Perfect" semi-infinite linear diffusion, i.e., diffusion occurring in one dimension bound by the planar electrode side, can be described by a Warburg element only when the phase angle is 45° in the low-frequency region. In other cases, when a low-frequency tail shows deviation from a 45° angle, a CPE with n different but close to 0.5 is usually employed [58].

The overall EIS data indicate that the corrosion behaviour of Zn-ZrCC is predominantly influenced by diffusion rather than charge transfer. The inherent instability of Zn, observed by fluctuations already during OCP measurements followed by low-frequency fluctuations during EIS measurements, introduces further errors in subsequent PPC measurements, compounded by their destructive nature. Thus, Zn-ZrCC behaviour, influenced by mass-transport control, is more accurately delineated through EIS than PPC, as Tafel extrapolation is inherently apt for describing activation processes [86]. Additionally, the absence of diffusion control in ORR regions of subsequent PPCs of Zn could imply

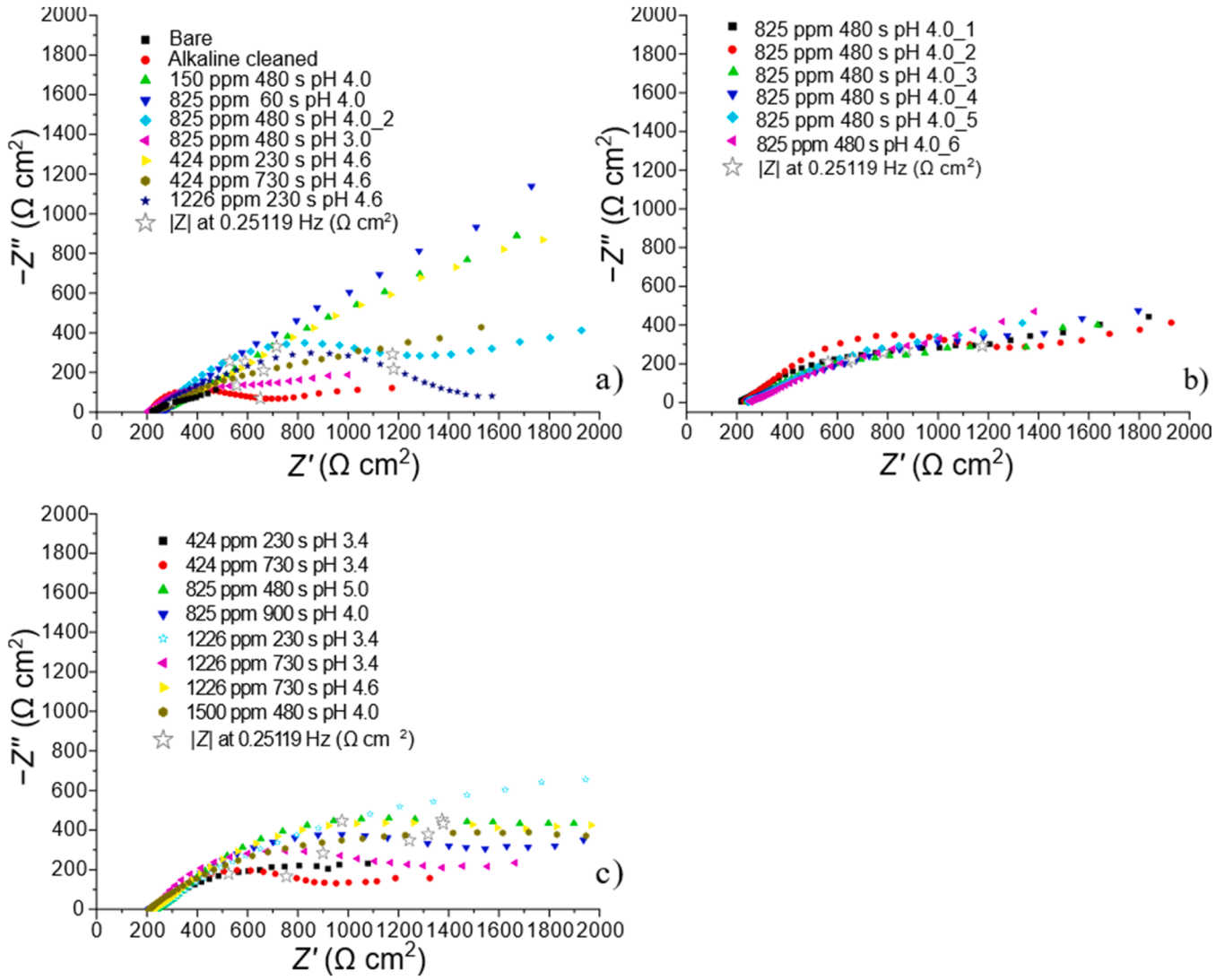

Fig. 4. EIS results for Zn-ZrCC in dilute Harrison's solution: (a) chosen results for discussion, (b) results of central point repetitions, (c) results obtained under the remaining conditions. Bare and alkaline-cleaned substrates are presented in (a). Rest periods at OCP were 300 s.

the diffusion of corrosion products, rather than oxygen or hydrogen, from the bulk electrolyte.

3.3. RSM results

Results obtained for thin films are often within the same order of magnitude, leading to statistically unreliable data. By employing a larger sample size, such as in RSM, the statistical test's power can be increased, making it easier to detect statistically significant differences [10–12,87], which was the very purpose of this study. Respected ZrCC results are compared to bare and chemically pretreated samples, both referred to as ZrCC-free samples. Table 2 summarises the input parameters of non-electrochemical and electrochemical methods for RSM. To reiterate, the PA of both substrates was assessed after exposure to 80 °C and, additionally, after 24 hours of air-drying at room temperature on Zn. A threshold for a good PA value for each substrate was estimated to be higher than the last applied ZrCC pretreatment (3.3.1.1). R_p obtained from EIS was used for CRS as the only electrochemical response. In contrast, $|Z|$ at 0.25119 Hz from EIS, along with j_{corr} and R_p obtained from Tafel extrapolation, were used as responses for Zn after 24 hours of air drying (Table 2)[2]. RSM results will be further discussed, focusing on the most significant parameters as indicated by F-values,[3] with higher values showing a greater influence on the response. Further explanations are given in Supplement, Sections 1 and 3.

3.3.1. RSM for protective ability

3.3.1.1. Cold-rolled steel. Based on ANOVA analysis in the Supplementary material, Section 3, it can be inferred that the model for the PA after 10 minutes is significant, with the lack of fit being insignificant.[3] All three parameters were found to have an effect, either the main or interaction, as shown in Eq. 1.

The response surface equation in terms of actual factors for PA after

[3] The F-value in an ANOVA is calculated as: variation between sample means / variation within the samples. The higher the F-value, the higher the variation between sample means relative to the variation within the samples. The coefficient of determination (R^2) is a number between 0 and 1 that measures how well a statistical model predicts an outcome. The lack of fit test assesses whether the chosen model adequately represents the relationship between the factors (independent variables) and the response (dependent variable). If the replicates have been run correctly, a significant lack of fit indicates that the model may not be fitting all the design points well.

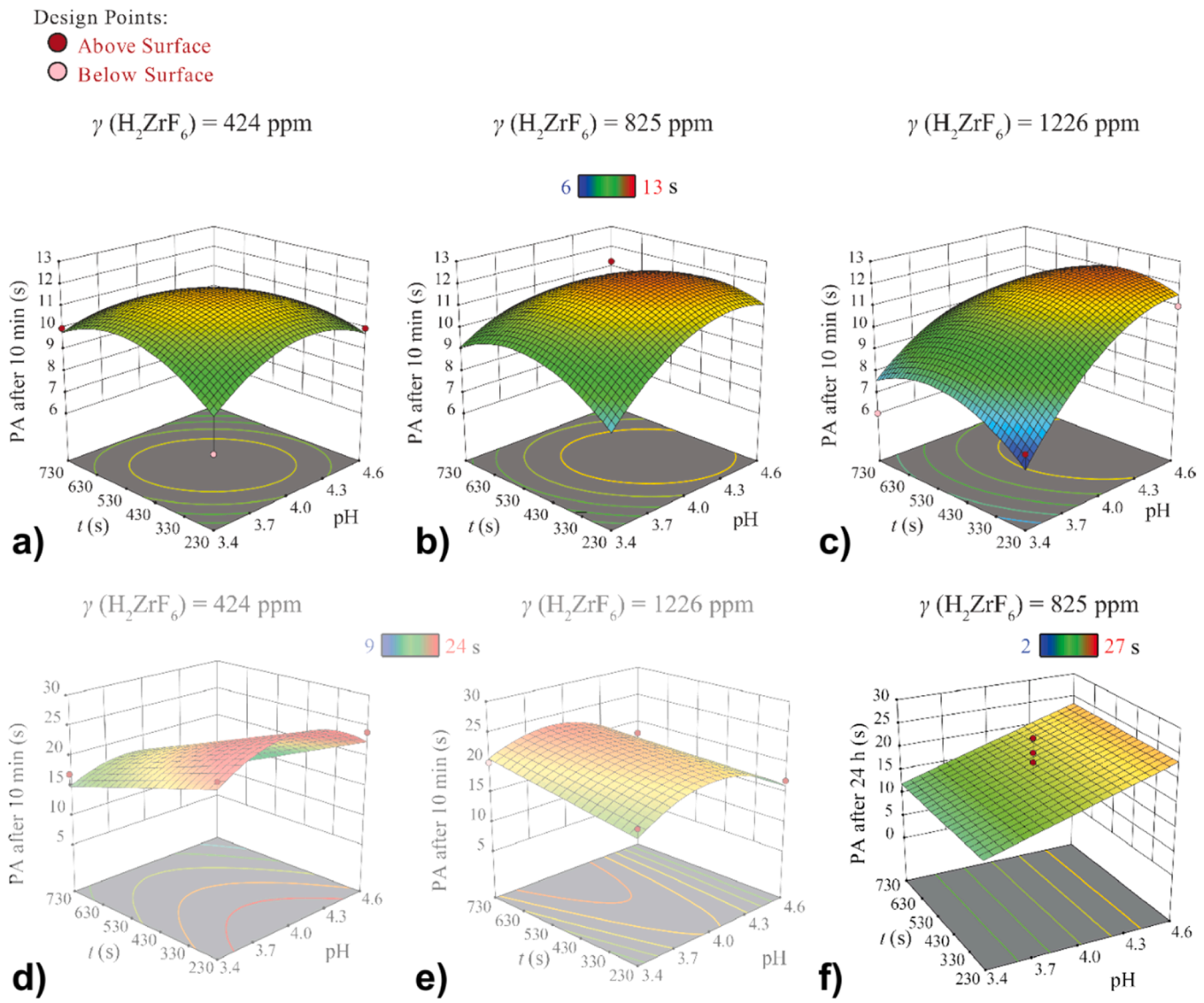

Fig. 5. RSM plots for PA of ZrCCs: (a-c) PA after 10 min on CRS for γ (H_2ZrF_6) of 424, 825 and 1226 ppm, (d,e) PA after 10 min on Zn for γ (H_2ZrF_6) of 424 and 1226 ppm, and (f) PA after 24 h on Zn for $\gamma(H_2ZrF_6)$ of 825 ppm. The extent of results is represented on colour scales above the graphs. Measured points denoted by red and pink circles are located above or below predicted values, respectively. Reliability of the RSM models: very reliable: PA after 10 min on CRS (a-c) and PA after 24 h on Zn (f). Insufficiently reliable: PA after 10 min (d,e); images were shaded to notify their unreliability.

10 min on CRS is given in Eq. 1:

$$\text{PA after 10 min / s} = -54.43485 + 29.96020 \times \text{pH} + 0.03888 \times \text{t} + -0.01326 \times \gamma - 0.004768 \times \text{pH} \times t + 0.0043660 \times \text{pH} \times \gamma - 3.729082 \times \text{pH}^2 - 0.000021 \times t^2 - 0.0000027 \times \gamma^2 \quad (1)$$

Furthermore, based on p- and F-values, the two most significant model terms are the quadratic terms of pH and time. However, this model also detects significant parameter interactions between pH and conversion time, as well as pH and concentration. R^2 and adequate precision values confirm that the model is highly reliable.

Eq.1 translates to RSM plots for CRS-ZrCCs in Fig. 5a,b,c and RSM matrix in Table S5.[4] It is observed that the best performance of ZrCCs based on the drop test is in the middle to higher concentrations (825−1226 ppm) as well as middle to higher pH values (4.0−4.6) and middle conversion times (480 s), suggesting that the optimum has already been reached in the central point (825 ppm, pH 4.0 and 480 s).

Due to the nature of this method, the exact determination of the point at which the colour changes may be relatively subjective, although its hue is less subjective and would, among other requirements, necessitate the test to be run by several persons independently. Therefore, it can be summarized that for CRS, optimal PA values are near the central point of middle to higher concentrations, conversion time and pH.

3.3.1.2. Zinc. Based on ANOVA analysis in the Supplementary material, Section 3, it can be inferred that the PA after 10 minutes model is significant, although with a very low F value, with the lack of fit being insignificant, albeit with a relatively low probability. All three parameters were confirmed to be significant, and, based on p- and F-values, the two most significant model terms were quadratic terms of pH and an interaction term between pH and concentration, followed by a linear term of conversion time. However, the low probability of the lack of fit, as well as slightly lower than required R^2 and tightly sufficient adequate precision values, confirm that the model is not reliable.[3] Therefore, the equation for this model is not given, although the response surface

[4] In RSM plots, above-design points refer to measured values that exceed the predicted surface, whereas below-design points indicate values falling beneath them, representing a disparity between predicted and actual observations.

(Fig. 5d,e with RSM matrix in Table S6) is presented to help readers visualise the response, which is invalid and, therefore, not a good evaluation metric herein. This unreliability translates in Fig. 5d-f to the existence of two optimal regions, the first moving from lower concentrations and lower conversion times toward higher concentrations and higher conversion times with a slight curvature at the middle pH value (4.0), giving inconclusive and misleading conclusions. These RSM models in Fig. 5d,e are shown only to demonstrate the unreliability of this parameter to obtain conclusive results.

On the other hand, based on ANOVA analysis in the Supplementary material, Section 3, it can be inferred that the model for PA after 24 hours is more significant compared to the previous model for the PA after 10 minutes, with the lack of fit being insignificant, along with reasonably high R^2 and adequate precision values point that the model is moderately reliable. However, based on both p- and F-values, the only significant model term is pH, and as such, this model can only be used to guide the experimental space to higher pH. The response surface equation in terms of actual factors for PA after 24 h on Zn is given in Eq. 2:

$$\text{PA after 24 h / s} = -20.33557 + 9.52139 \times \text{pH} \quad (2)$$

Eq. 2 translates to RSM plots in Fig. 5f that show the PA after 10 min response (Fig. 5d,e) resolving after 24 h. This is a direct result of a considerable decrease in PA for samples with pH < 4.0, in contrast to the improvement seen in samples with a pH ≥ 4.0, most probably due to the formation of ZnO filling in the pores.

Furthermore, the growth of native oxide within presumed pores developed in ZrCCs during electrolyte exposure could enhance the overall corrosion resistance of ZrCCs. This approach is supported by the long-established Pilling-Bedworth ratio [73], which indicates the development of protective oxides for zinc but not for iron. In fact, leaving ZrCCs on CRS in the air leads to rusting [88], while a significant improvement of ZrCCs has been observed before on aluminium alloy substrates and Zn, either by allowing for native oxide development on air or by leaving in the electrolyte for 24 h [14,15,61,62].

It can be summarized that for Zn, PA after 10 minutes is not a confidential evaluation response. However, PA after 24 hours, although having pH as the only influential parameter, can provide better predictions for characterisation by navigating the experimental space toward higher pH values.

3.3.2. RSM for corrosion current density on Zn

Based on ANOVA analysis in the Supplementary material, Section 3, it can be inferred that the model is significant, albeit with a very low F value; however, the lack of fit is also significant. Based on p- and F-values, the two most significant model terms for j_{corr} are the quadratic terms of pH and conversion time. However, the significant lack of fit, despite sufficient R^2 and adequate precision values, points to the fact that the model is not reliable. However, the response surfaces in Fig. 6a-c are presented herein as they depict the obtained data but cannot be used for characterisation or optimisation.

From Fig. 6a-c and Table S6, it is seen that the lowest corrosion current density values are obtained at middle concentration (825 ppm), middle conversion time (480 s), and middle pH levels (4.0). However, this minimum value increases as the concentration rises towards lower pH values, resulting in a somewhat inconclusive trend. A higher variability between the experimental and predicted values also accompanies this observation, as seen in the Supplementary material, Section 3.

These results overall imply that j_{corr} might not be the most appropriate parameter for evaluating Zn-ZrCC performance, even though it accurately depicts the obtained data.

3.3.3. RSM for polarisation resistance from Tafel extrapolation on Zn

Based on ANOVA analysis in the Supplementary material, Section 3, it can be inferred that the model for R_p Tafel extrapolation is significant, although with a very low F value, with the lack of fit being insignificant. All three factors were found to have an effect, either the main or interaction, as shown in Eq. 3; however, based on F-values, the two most significant model terms are the quadratic terms of pH and interaction term between pH and concentration. Moderately high R^2 and adequate precision values suggest the model is moderately reliable, a bit better than that for corrosion current density.

The response surface equation in terms of actual factors for R_p Tafel extrapolation on Zn is given in Eq. 3:

$$R_p \text{ Tafel extrapolation / } \Omega\,\text{cm}^2 = -11549.00877 + 5801.10995 \times \text{pH} + 2.11536 \times t + 4.96291 \times c - 1.27656 \times (\text{pH} \times c) - 565.00305 \times \text{pH}^2 - 0.002798 \times t^2 \quad (3)$$

Eq. 3 translates to RSM plots in (Fig. 7a-c and Table S2), showing the predicted optimum for R_p at lower concentrations (424 ppm) coupled with higher pH (4.6) and shorter conversion times (230 s). There is a noticeable decline in the response with an increase in concentration (825 ppm), yet the trend concerning pH and conversion time is maintained, distinguishing it slightly from the results obtained for j_{corr}.

It can be inferred that R_p from Tafel extrapolation has the potential to

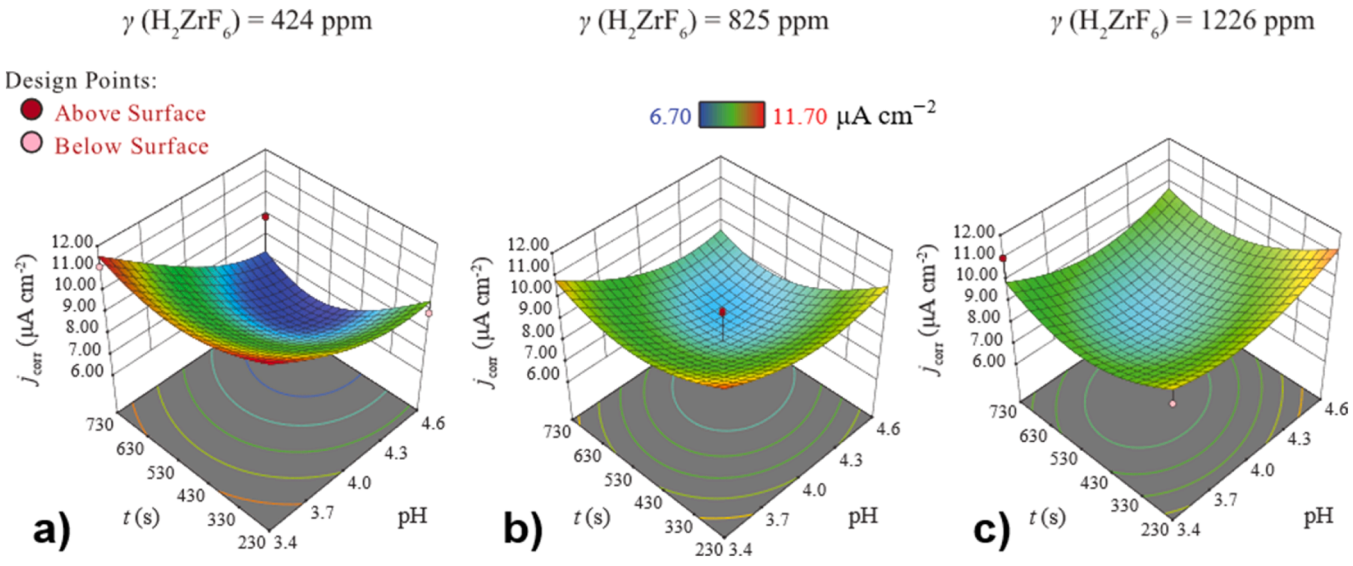

Fig. 6. RSM plots for Zn-ZrCCs for j_{corr} from PPCs for γ (H_2ZrF_6) of 424, 825 and 1226 ppm (a-c). The extent of results is represented on colour scales above the graphs. Measured points denoted by red and pink circles are located above or below predicted values, respectively. Reliability of the RSM model: unreliable.

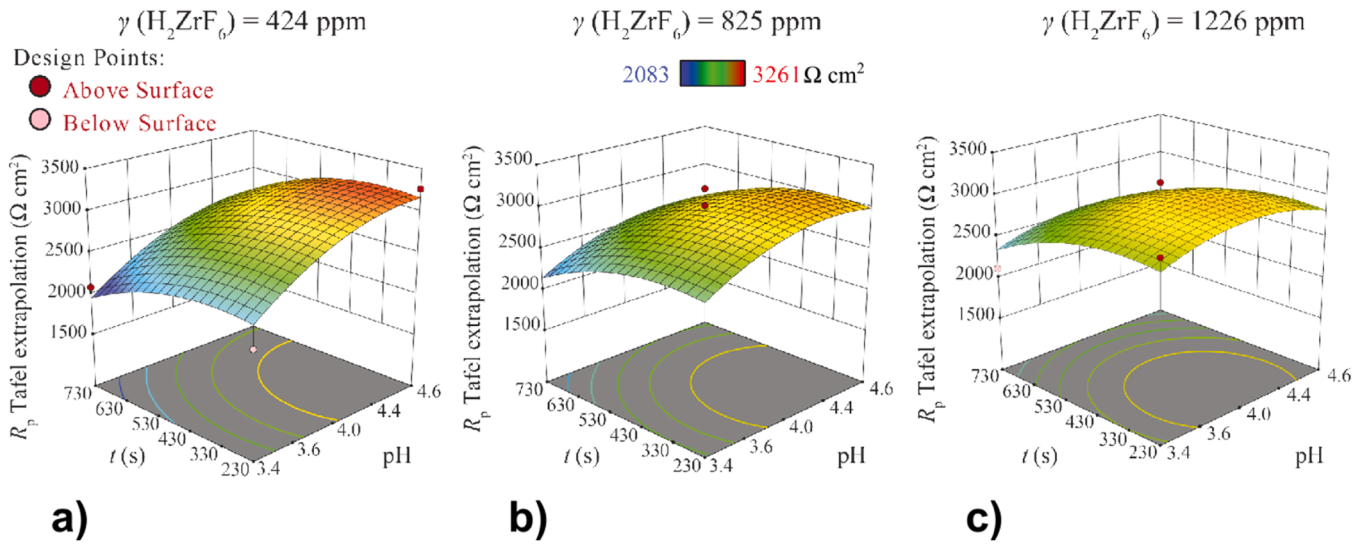

Fig. 7. RSM plots for Zn-ZrCCs for R_p Tafel for γ (H_2ZrF_6) of 424, 825 and 1226 ppm (a-c). The extent of results is represented on colour scales above the graphs. Measured points denoted by red and pink circles are located above or below predicted values, respectively. Reliability of the RSM model: sufficiently reliable.

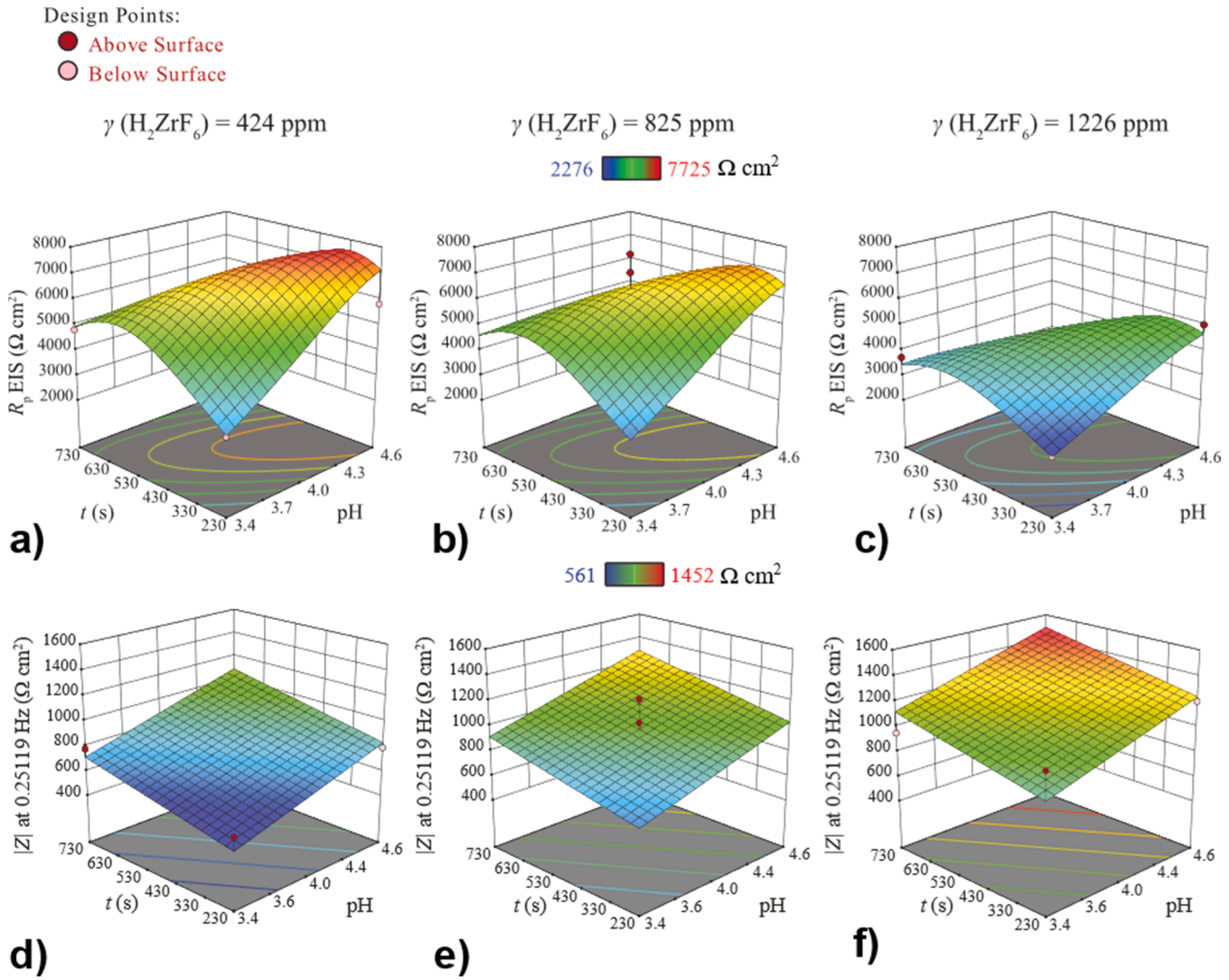

Fig. 8. RSM plots for EIS responses of ZrCCs: (a-c) R_p EIS on CRS and (d-f) $|Z|$ at 0.25119 Hz on Zn for γ (H_2ZrF_6) of 424, 825 and 1226 ppm. The extent of results is represented on colour scales above the graphs. Measured points denoted by red and pink circles are located above or below predicted values, respectively. Reliability of the RSM models: very reliable.

be a more suitable metric for PPC measurements than j_{corr}. Indeed, it has been shown to fit the model in contrast to j_{corr}.

3.3.4. RSM for EIS results

3.3.4.1. Cold-rolled steel. Based on ANOVA analysis in the Supplementary material, Section 3, it can be inferred that the model is significant, with the lack of fit being insignificant. All three parameters were found to have an effect, either the main or interaction, as shown in Eq. 4. However, based on p- and F-values, the two most significant model terms for R_p EIS are the quadratic terms of pH and conversion time. This model also detects significant parameter interactions between pH and conversion time. R^2 and adequate precision values confirm the high reliability of the model.

The response surface equation in terms of actual factors for R_p from EIS on CRS is given in Eq. 4:

$$(R_p \text{ EIS})^{-0.5} / \Omega \text{ cm}^2 = 0.10729 - 0.03393 \times \text{pH} - 0.00010 \times t - 5.69886\times10^{-6}) \times \gamma + 1.65388\times10^{-5} \times \text{pH} \times t + 0.00311 \times \text{pH}^2 + 3.87861\times10^{-8} \times t^2 + 5.56393\times10^{-9} \times \gamma^2 \quad (4)$$

RSM plots for R_p on CRS described by Eq. 4 are shown in Fig. 8a-c with RSM matrix in Table S3. These results suggest a trend towards lower concentrations and higher pH levels, even though the measured values in that range were not as high as at the central point, i.e., 825 ppm/480 s/pH 4.0 (Table S5). However, it can be inferred that the best performance has already been reached at the central point after accounting for the impact of its variability estimated from ANOVA, shown by the contrast between predicted and repeated measured central points. EIS seems to exhibit a higher sensitivity to the concentration effect than the drop test and, in fact, to all other factors and their interactions. This is evidenced by the accompanying F-values for specific model terms in Supplementary material, Section 3.

3.3.4.2. Zinc. Based on ANOVA analysis in the Supplementary material, Section 3, it can be inferred that the model for $|Z|$ at 0.25119 Hz is significant, with the lack of fit being insignificant. All three parameters were found to have an effect, either the main or interaction, as shown in Eq. 5, with the most significant model term being the linear term of concentration, followed by pH, and lastly, conversion time. R^2 and adequate precision values confirm that the model is highly reliable. The response surface equation in terms of actual factors for $|Z|$ at 0.25119 Hz on Zn is given in Eq. 5:

$$|Z| \text{ at } 0.25119 \text{ Hz} / \Omega \text{ cm}^2 = -815.78636 + 276.53202 \times \text{pH} + 0.422036 \times t + 0.564076 \times c \quad (5)$$

The derived RSM surfaces from Eq. 4 expressed as $|Z|$ at 0.25119 Hz (Fig. 8d-f and Table S6) diverge from their previously discussed responses in the context of Zn, indicating an optimum at higher concentrations (1226 ppm), longer conversion times (730 s), and higher pH (4.6). This suggests the sensitivity of EIS to reflect ZrCC resistance due to the effect of longer conversion time on increased thickness.

3.3.5. Comments on the overall feasibility of RSM models for CRS and Zn

The statistical analysis of RSM models from the Supplementary material, Section 3, suggests that all models can be used to navigate the experimental space. However, for CRS, the PA after 10 minutes model is good for characterisation, and the R_p EIS model is useful for both characterisation and, possibly, optimisation. This is expected due to EIS's inherent higher sensitivity to subtle changes in electrochemical processes. For Zn, the PA after 10 minutes, j_{corr}, and R_p Tafel extrapolation models are not suitable. However, the PA after 24 hours and $|Z|$ at 0.25119 Hz models are effective for both characterisation and optimisation. The fact that the feasibility of certain responses varies with the substrate complicates the optimisation of both substrates and their individual responses. Only EIS arises as a mutual evaluation technique suitable for both characterisation and optimisation of these substrates. However, care must be taken in choosing the type of resistance as a response, as it differs between the two substrates.

3.4. Surface analysis by SEM/EDS

After building an empirical model from RSM and estimating the main and possible interaction effects of particular factors, the most research-compelling samples were subjected to SEM analysis to argue particular RSM response results.

For discussional purposes, only Zr, O, and Fe contents obtained by EDS were found relevant. The atomic percentages of these elements are provided alongside the locations where EDS spectra were acquired on SEM micrographs in Figs. 9–11. Complete EDS analyses can be found in the Supplementary material, Section 4 (Figs. S4-S5). The coating density has a large impact on electron penetration depth. In a practical setting, the density may be notably reduced, leading to a faster arrival of the beam at the substrate, which impedes quantitative determination of light-weight elements, such as O. Our Monte Carlo simulations (not shown) reveal that on Zn and CRS, the penetration depth is 60 nm at 3 kV, 230 nm at 5 kV, and 1560 nm at 15 kV, assuming a model thickness of 20 nm.

Furthermore, considering peak overlapping, especially that of F and Fe [89], assessing the quantitative impact of concentration and conversion time on ZrCC thickness is unreliable [90,91]. Nevertheless, both thickness and coating density can be indirectly inferred[5].

3.4.1. Cold-rolled steel

Fig. 9 shows that a clean bare surface exhibits a nanometric-sized fine structure [18], which is presumably just grinding residues, as indicated by the same Fe and O content throughout the whole surface. Alkaline cleaning (pH=7.4) changes the surface morphology of the substrate to nanometric lamellar and nodular structures. Increased O content suggests that FeO formation may occur [92] during alkaline cleaning if adequate OCP is achieved, as indicated in our recent study [45]. Commenting on O content is uncertain for the reasons mentioned above. However, it can be used for comparative purposes in cases where the difference exceeds an order of magnitude.

Fig. 9 also shows that all ZrCCs on CRS uniformly follow the topography of the underlying substrate, exhibiting nodular morphology [93]. Uniform coating formation can be ascribed to uniform corrosion [86], where the location of anodic and cathodic sites changes continuously due to small changes in surface reactivity as the corrosion process proceeds. The sample prepared at the shortest conversion time, 825 ppm/60 s/pH 4.0, shows low Zr content and morphology similar to the underlying morphology caused by alkaline cleaning. However, extending the conversion time from 60 to 480 s leads to an increase in Zr content along with a Fe content decrease, indicating an increase in coating thickness.

On the other hand, the effect of pH is stricter. The sample subjected to the lowest pH (3.0) exhibits almost no Zr (at least not detectable by EDS) and significantly decreased O content at the coating's bulk (site #1) with only rarely distributed zirconia particles (site #2) over the surface and surface morphology similar to the underlying substrate, i.e. alkaline cleaned sample. However, moving pH to slightly less acidic (3.4) and a slightly higher concentration (1226 ppm) (and accordingly shorter conversion time of 230 s) reveals at least some coating formation over the whole surface, although with a very low Zr content (Fig. S4) and the overall morphology similar to the alkaline cleaned surface. From

[5] To achieve an accurate evaluation of F content, advanced techniques such as wavelength dispersive X-ray analysis (WDX) with superior energy resolution are necessary to prevent common peak overlap errors encountered in EDS analysis. Consequently, the enclosed EDS results are only semi-quantitative [90, 91].

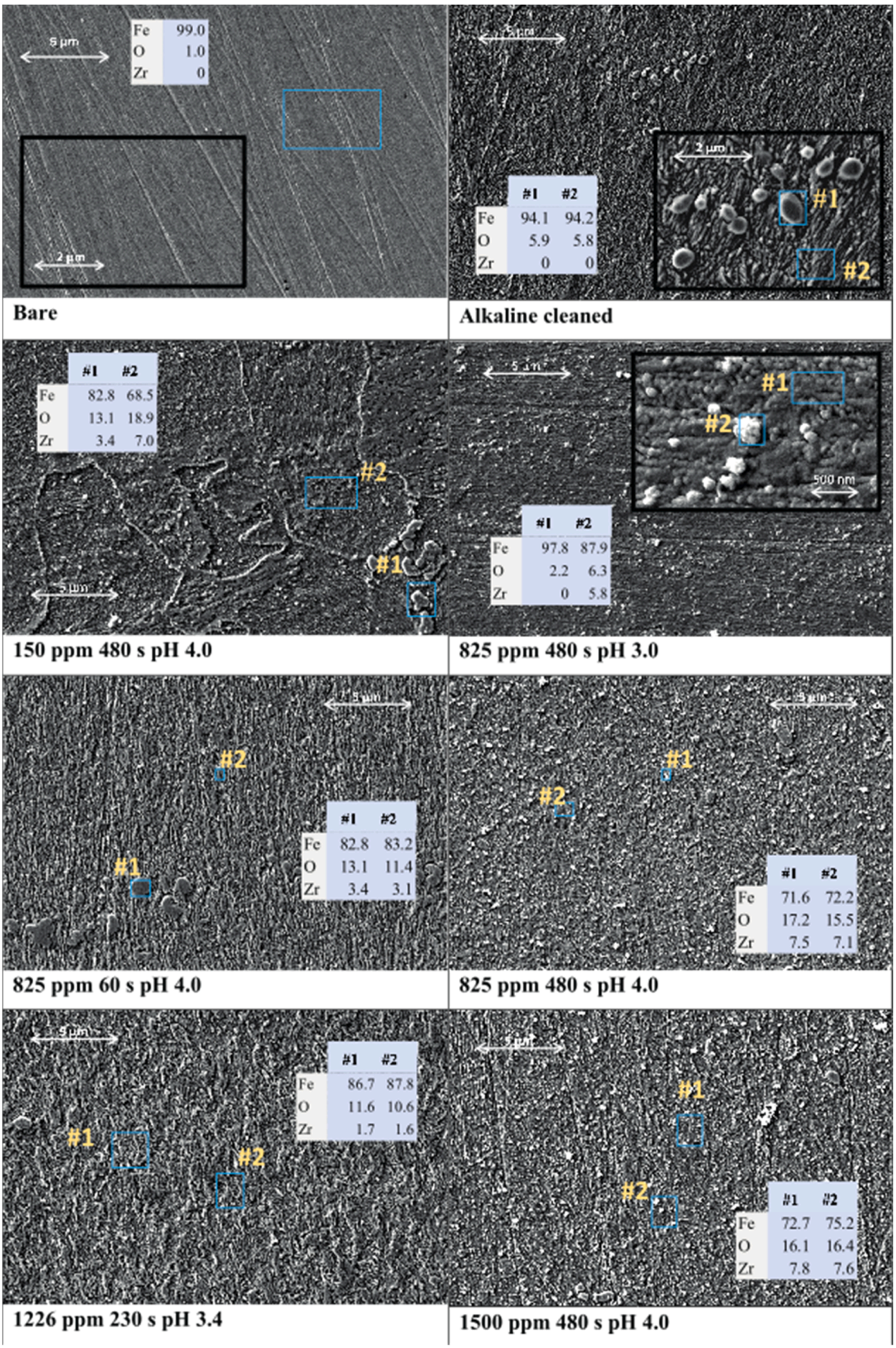

Fig. 9. SEM micrographs of bare and alkaline-cleaned CRS samples and CRS samples subjected to various ZrCC treatments. The sites of EDS analyses are noted by blue rectangles, and the results for Fe, O and Zr are given in tables inside the images. All EDS results are given in Supplementary material, Section 4.

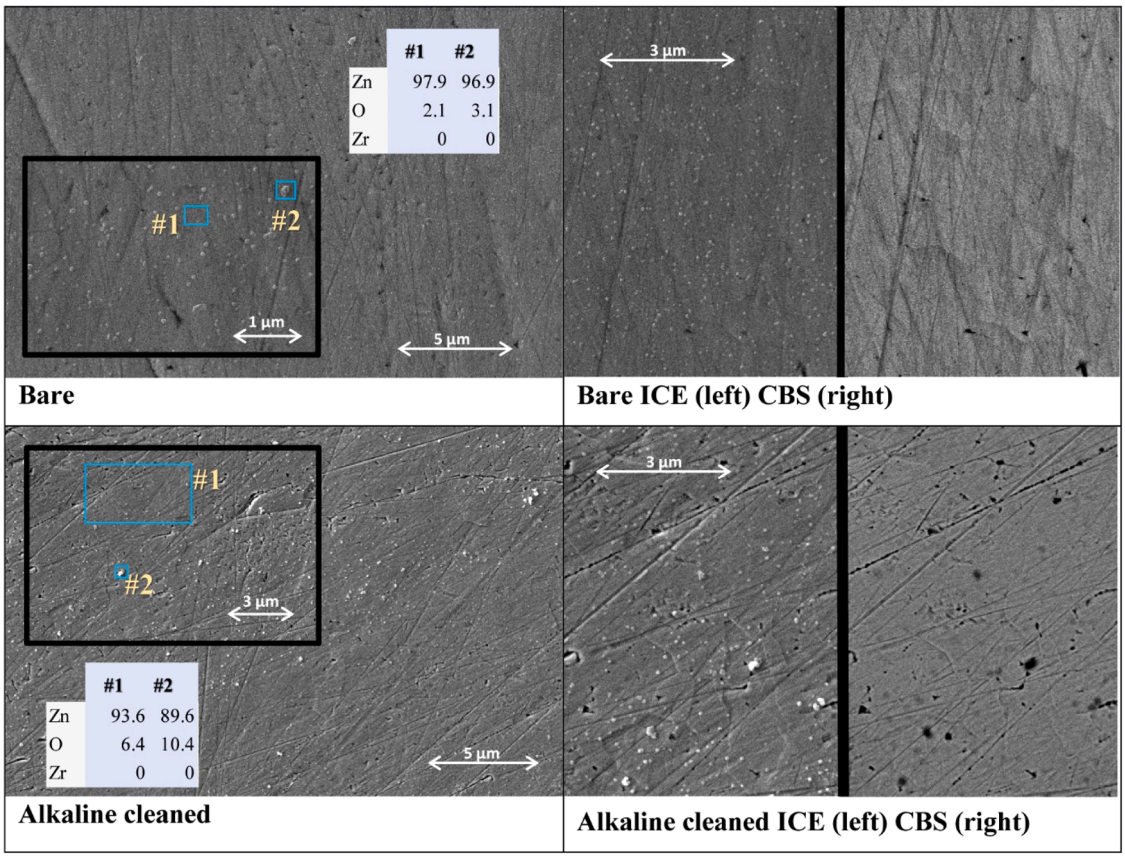

Fig. 10. SEM micrographs of bare and alkaline-cleaned Zn ZrCC-free samples. Blue rectangles note the sites of EDS analyses, and the results for Zn, O and Zr are given in tables inside the images. Micrographs on the right side were captured using the CBS detector mode to confirm the presence of oxide further. All EDS results are given in Supplementary material, Section 4.

this, it can be inferred that pH $<$ 4.0 leads to an insufficient coating formation, although at some spots, a sufficient rise of pH for ZrCC precipitation is probably achieved even under those conditions, as indicated by a low amount of Zr detected. This is explained by a much higher corrosion rate of iron and steel at pH $<$ 4.0 caused by a greater effect of HER accompanying oxygen reduction reaction (ORR), as well as the fact that ferrous oxide, FeO (that should otherwise form and remain stable during alkaline cleaning), is soluble at pH $<$ 4.0.

The above-described observations of insufficient coating formation are confirmed through EIS spectra, as only one time constant is observed with the shape and width of the capacitive loop, similar to ZrCC-free samples (Fig. 3a). However, only at extended conversion times (730 s) with such concentration setting, an HF loop appears in EIS spectra, indicating thickening of the ZrCC layer. From this, it can be inferred that pH $<$ 4.0 generally leads to an insufficient coating formation, which can only be compensated with a combination of higher concentration (1226 ppm) and longer conversion time (730 s). On the other hand, samples prepared at pH $\geq$ 4.0 exhibit sufficient coating formation, as indicated by three time constants (3.2.2.1). Hence, the high-frequency time constant can indeed function as an indicator of adequate ZrCC formation. In addition, the occurrence of the high-frequency time constant completely coincides with PA values above 10 s, meaning that PA, although inherently less sensitive and more subjective, can actually serve as a very fast screening method for indication of sufficient ZrCC formation on CRS. Our recent research has demonstrated that an adequate formation of ZrCC requires a minimum pH of 4.0. At this pH, a polymeric Zr film, including the tetrameric form, can form, whereas a pH of 3.0 results only in the formation of dimeric species [94].

The beam depth does not allow for differentiation between Zr content when performing conversion at different H_2ZrF_6 concentrations at the same pH and time setting (pH $>$ 4.0). Still, the samples 150 ppm/480 s/pH 4.0 and 825 ppm/480 s/pH 4.0 exhibit similar Zr contents, but the obtained topography for the former is similar to the underlying substrate, whereas a thicker layer is formed for the latter, i.e., at higher concentrations. Similarly, although not reflected in higher Zr content, the sample prepared at the highest concentration, 1500 ppm, shows higher Zr nodule density, suggesting either higher thickness or compactness. However, it has already been established that after immersion in the electrolyte, thicker conversion coatings are more prone to cracking [95–99] and can lead to delamination of the subsequent topcoat [100] due to internal stress buildup. This is reflected in the best-performing value rather at the centre of the chosen experimental space, i.e., 825 ppm/480 s/pH 4.0 towards higher concentrations (1226 ppm) and pH (4.6) (Fig. 5a,c and Fig. 8a-c) and not at 1500 ppm from EIS. This also supports the previous study on CRS, where the coating formations were promoted at pH 4.0 due to establishing a dynamic equilibrium between dissolution and precipitation [101].

3.4.2. Zinc

The bare Zn surface also shows a few grinding residues, confirmed through EDS analysis, having almost the same Zn content throughout the surface (Fig. 10). After alkaline cleaning, the surface is covered with nodular ZnO. This is confirmed by higher concentrations of Zn and O at the nodular locations, and darker circles observed when using the CBS detector mode, all of which align with the expected results for the given pH (12.5), Fig. S5.

All Zn-ZrCC samples underwent morphological changes resembling chipping to varying extents due to acid etching. These changes are otherwise highly dependent on the solution composition and are particularly noteworthy in the design of Zn anodes [102].

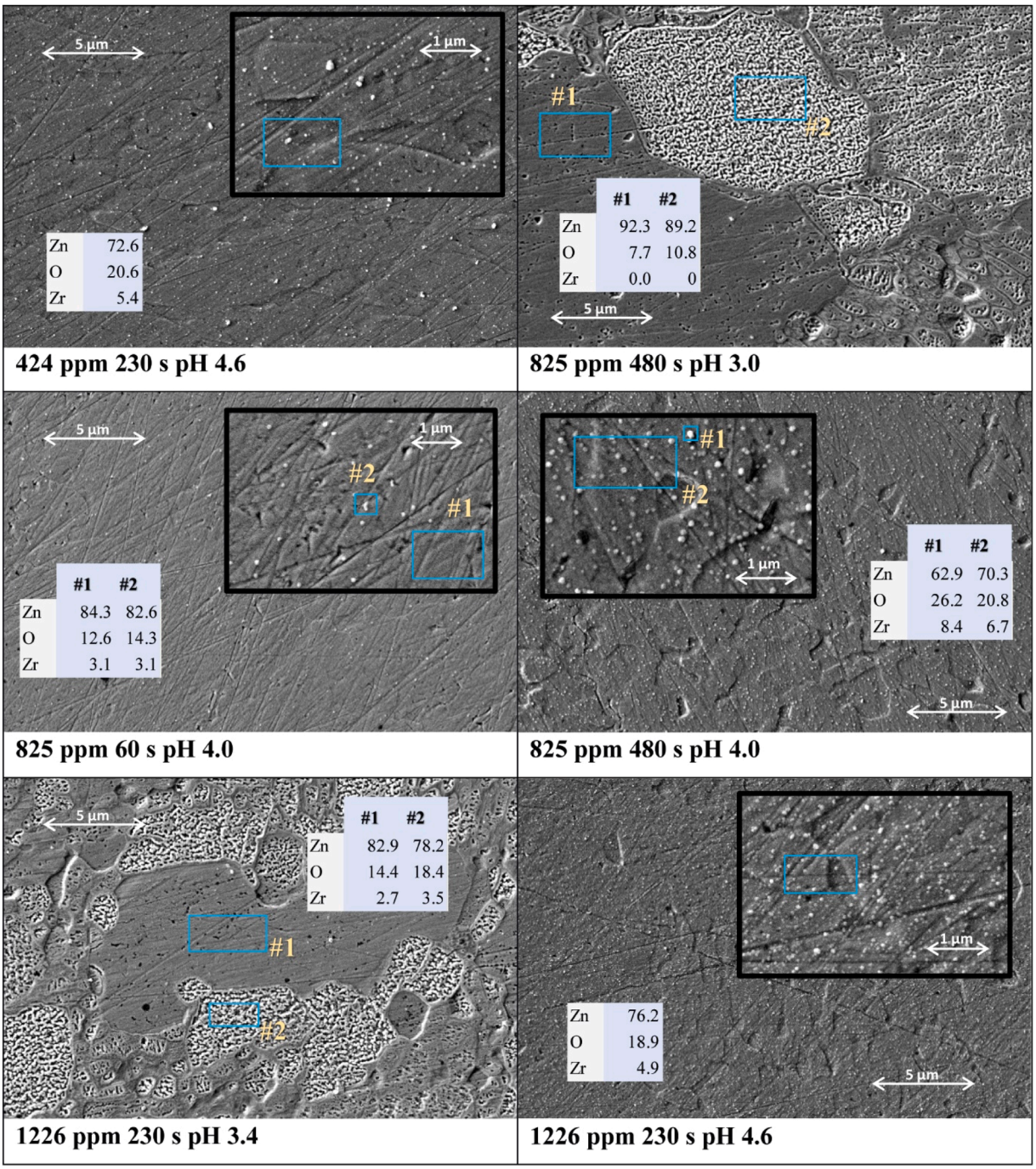

Fig. 11. SEM micrographs of Zn ZrCC-free samples prepared under different conditions. Blue rectangles note the sites of EDS analyses, and the results for Zn, O and Zr are given in tables inside the images. All EDS results are given in Supplementary material, Section 4.

Like CRS, ZrCC on Zn exhibits nodular morphology, with the population of nodules, in general, increasing with an increase in either conversion time and H_2ZrF_6 concentration. In the case of Zn, the effect of low pH was the most prominent, where pH < 4.0 leads to excessive etching of the surface (Fig. 10), revealing bare Zn regions and highly nodular ZnO regions. This is due to the cathodic control of HER leading to significantly higher corrosion rates on Zn below pH 4.0. In mildly acidic solutions, which accounts for pH 4.0, due to lower concentration of H^+, the influence of otherwise a large overpotential of HER on Zn prevails and shifts cathodic control to ORR, which, due to a fixed oxygen concentration, leads to almost constant corrosion throughout a wide subsequent pH range [103]. However, it should be noted that the conversion process appears to be influenced not only by pH but also by the conversion agent; for instance, molybdate conversion coatings exhibit faster deposition at pH 3.0 [104]. Interestingly, while the sample 825 ppm/480 s/pH 3.0 was only etched without any detectable ZrCC formation, the sample 1226 ppm/230 s/pH 3.4, although extensively etched, still did form a thin ZrCC layer, as indicated by low Zr content (Fig. 11). This is probably a compromise of slightly lower corrosion rates at a slightly less acidic pH of 3.4, compared to 3.0, enabling ZrCC deposition to occur, although in a very small amount. Only conversion at pH ≥ 4.0 led to uniformly coated surfaces (Fig. 11). Furthermore, based on RSM results for PA (Fig. 5d-f, Table S6), Zn samples treated at pH < 4.0 showed some PA values already after 10 minute test, which

decreased after 24 hours, while ZrCC-free Zn samples showed PA only after 24 hours. Combining with EIS and SEM results, this may suggest that an etched surface rich in ZnO with higher geometry and possible hydrophobicity, along with some ZrCC formation, leads to PA>0 in those samples. However, this effect resolves after 24 hours as the acidic environment within pores from the ZrCC process deteriorates the surface, leading to lower PA values than ZrCC-free Zn samples.

A higher pH and higher concentrations generally lead to a thicker coating, as evidenced by higher Zr content. In addition, higher concentrations led to more ZrCC nodules on the surface (Fig. 11). However, the shape of low-frequency arcs (Fig. 4) ascribed to diffusional processes in the case of Zn shows consistent trends that can be useful for Zn-ZrCC evaluation when immersed in DHS.

Bare Zn and samples having thinner ZrCCs had very large low-frequency arcs (and consequently, large diffusion resistances, R_d) as a result of longer diffusion paths (Fig. 4a-c). On the other hand, alkaline cleaned and samples having higher ZrCC thickness, along with etched samples treated at pH < 4.0, exhibited lower low-frequency arcs due to shorter diffusion paths. This points to the fact that thicker ZrCC coatings resulted in the formation of less Zn corrosion products and vice versa. In addition, Zn corrosion products on bare Zn are more dense and thicker than the alkaline-cleaned sample that already had a thin and homogeneous layer of ZnO on it (compare Figs. 10 and 11). In contrast, samples deposited at pH < 4.0 had a highly accessible surface roughened by highly porous, inhomogeneously distributed nodular ZnO. This also enabled faster diffusion, reflected in lower R_d and R_{ct} values than Zn-ZrCC samples at pH ≥ 4.0.

It can be inferred that, in general, Zn-ZrCCs at pH ≥ 4.0, either at conversion times ≥ 230 s or concentrations ≥ 825 ppm, have higher coating thickness compared to those treated at lower settings of those factors. Thus, the width of the low-frequency arc associated with diffusion can indicate the degree of formation of Zn corrosion products, which is inversely proportional to ZrCC thickness. This implies a greater long-term predictive capacity for EIS, recognizing the influence of prolonged conversion time on thickness increase, resulting in improved corrosion resistance. This contrasts R_p derived from Tafel extrapolation (Fig. 7), which places more emphasis on lower concentrations and shorter conversion times; the latter were indeed found less suitable according to RSM models. However, it is noteworthy that all samples treated at pH 4.0 and concentration exhibit similar values in $|Z|$, supporting the effect of ZrCC thickness on its corrosion resistance. However, it remains unresolved why the sample at 1224 ppm/230 s/pH 4.6 seemingly exhibits the least diffusion control, suggesting the most resistive ZrCC film, which may not necessarily be related to thickness but possibly to compactness.

3.5. Critical assessment of ZrCC's deposition performance on cold-rolled steel and zinc

The final choice of responses for use in the RSM was determined during the initial experimental combinations of the RSM matrix. Specifically, the application of PA on Zn after 24 hours was introduced after observing a significantly improved response on the first day of RSM experiments when PA was applied for 10 minutes. The use of PPC on Zn was decided upon after preliminary observations showed an anodic shift in CRS. The decision to use $|Z|$, and particularly at $|Z|$ at 0.25119 Hz instead of R_p on Zn, was made after completing all the RSM matrix combinations. This choice was further supported by SEM analysis while attempting to find a connection between the observed EIS spectra and SEM images.

Overall, the best performance for ZrCC deposition on CRS and Zn, guided by uniform corrosion, occurs at moderate to high concentrations (825−1226 ppm) and pH levels of 4.0−4.6. Uniform coating formation on Zn and CRS results from continuous changes in local anodic and cathodic sites. For CRS, both RSM responses suggest a slight shift towards higher pH and concentrations with increased conversion time. Notably, the best protective coating can be achieved at lower pH levels, such as 3.4, with extended conversion time. This is further supported by EIS results, where samples under the same conditions but with extended conversion time (1226 ppm, 730 s, pH 3.4) exhibit a high-frequency loop, confirming the presence of a satisfactory coating. This suggests a balance between acidity, conversion time, and Zr availability near the surface at higher concentrations.

In the case of CRS, both model responses, i.e. PA after 10 min and R_p EIS, were found to be very reliable, leading to similar RSM surface shapes. However, the drop test primarily responds to variations in pH and the establishment of an adequate coating, yielding relatively consistent values in the latter scenario. However, the R_p EIS model was more sensitive to coating composition differences at varying concentrations, pH and conversion time, while the HF loop confirmed that sufficient coating formation was in line with higher PA values. Furthermore, the drop test was more sensitive for CRS and Zn at a pH < 4.0. For Zn, the drop test after air-drying for 24 hours primarily highlighted the influence of pH, indicating that a satisfactory coating forms at a higher pH (4.6), which is not necessarily related to its thickness. This is likely due to the inherent lower sensitivity of the drop test and the different reagents used compared to EIS, which still results in a sufficiently reliable RSM model. Nevertheless, similar to CRS, the EIS model was highly reliable for Zn. It can also indicate ZrCC thickness at pH ≥ 4.0 and reflect porous ZnO behaviour at pH < 4.0, as observed from SEM/EDS results. Additionally, current surface analysis data do not suggest porosity formation in dried ZrCC-coated samples at pH ≥ 4. Therefore, porosity is assumed to develop only during electrolyte exposure or due to excessive etching at pH < 4.

Nevertheless, to determine if the PA and R_p EIS models suggested optimal points, like 1224 ppm/230 s/pH 4.6, indeed outperform the central point in terms of drop test or EIS compatibility and to discern which method best characterizes ZrCCs for both substrates requires further investigation with more sensitive techniques like local electrochemistry, which are planned for the future research.

At the moment, it seems that only EIS has the potential to be used on both substrates for both characterisation and prediction/optimisation. In any case, RSM remains valuable for identifying the best conditions and elucidating complex relationships between input factors and responses, ultimately contributing to assessing the extent of viability of each evaluation technique.

It should be noted that DHS was primarily used in this study to simulate atmospheric conditions due to its presumed mild impact on the substrates of interest. However, caution is advised when applying DHS to other substrates and intermetallic particles, such as those based on Mg, where the presence of ammonium ions leads to dissolution and further formation of Mg complexes with sulfate ions, as demonstrated in previous studies [32].

4. Conclusions

This study utilised RSM to explore experimental conditions thoroughly, determine the best conditions, and assess factors of interactions on CRS and Zn substrates in various ZrCC bath conditions. In contrast to electrochemical methods, which produce quantitative parameters, PA measurements from the drop test are based on the relatively subjectively determined point of colour change. Hence, the drop test is recommended for a rapid initial assessment of ZrCC performance. Specifically, the drop test provides an accurate overview of ZrCC corrosion resistance on CRS after 10 min drying and on Zn after 24 hours.

In contrast, when using PPC, polarisation resistance proves more convenient than corrosion current density for evaluating performance; however, it is still not convenient enough to be used for optimisation.

Regarding electrochemical measurements, EIS emerges as the most sensitive method for analysing interactions between conversion bath parameters across diverse combinations. EIS results indicate that charge transfer resistance exclusively controls ZrCC corrosion behaviour on

CRS, whereas diffusion control prevails on Zn. However, EIS does not always reflect the overall corrosion resistance of ZrCC. On CRS, a high-frequency time constant in EIS spectra not only suggests higher corrosion protection but also indicates satisfactory ZrCC formation. Lastly, on Zn at pH $\geq$ 4.0, EIS effectively describes ZrCC thickness through the diffusion time constant, while at pH < 4.0, EIS captures the behaviour of the porous ZnO formed during conversion.

Nevertheless, in terms of the statistical applicability of the obtained RSM models, those derived from EIS can function as a universal approach for the characterisation and optimisation of these substrates, provided the selection of the appropriate type of resistance from EIS as a response is carefully considered.

What began with the goal of identifying optimal ZrCC conditions on various substrates has, due to observed problems, evolved into a study focusing on the feasibility of different evaluation techniques. Consequently, our study stayed in the characterisation/exploration phase, focusing on identifying main effects and interactions without advancing to the model-based prediction of optimal conditions, which would require further validation, representing the ultimate application of RSM. Yet, this methodological approach enhanced the reliability of findings and facilitated a seamless comparison of ZrCC performance across various substrates and its evaluation techniques, ultimately improving overall research credibility and laying the groundwork for future studies.

Author statement

All persons who meet authorship criteria are listed as authors, and all authors certify that they have participated sufficiently in the work to take public responsibility for the content, including participation in the concept, design, analysis, writing, or revision of the manuscript.

The authors declare that the science contained in this manuscript has not been previously published and is not under consideration by any other journal

Funding

This research was funded by the Slovenian Research and Innovation Agency (research core funding grants P2-0393 and P2-0266 and project PR-09806).

CRediT authorship contribution statement

Davorin Kramar: Writing – review & editing, Methodology, Conceptualization. **Ana Kraš:** Writing – original draft, Methodology, Formal analysis, Data curation, Conceptualization. **Ingrid Milošev:** Writing – review & editing, Supervision, Methodology, Funding acquisition, Conceptualization.

Declaration of Competing Interest

The author declare that they have no known competing financial interests or personal relationships that could have appeared to influence the work reported in this paper.

Acknowledgements

The authors acknowledge the funding agency (see Funding section). The authors sincerely thank Dr. Neil Spinner from Pine Research Instrumentation, Inc., for conducting insightful webinars, which were freely available and provided valuable knowledge. These sessions laid a strong foundation for deeper exploration of EIS literature and accurate interpretation of EIS spectra. Special gratitude is extended to Dimitrij Us, MSc, and Dr. Sabina Ovčjak from SurTec Adria d.o.o. for their generous guidance in preparing ZrCCs and sharing their invaluable industry expertise. Additionally, the authors appreciate Dr. Iosif Fromondi from Methrom Autolab for always being readily accessible for help and for his generous user support in utilizing Autolab and NOVA. His guidance in EIS fitting within NOVA has been invaluable. Finally, heartfelt thanks are extended to Barbara Kapun, BSc., Dept. of Physical and Organic Chemistry, for her prompt SEM/EDS analyses and engaging discussions. The authors acknowledge the Centre of Excellence in Nanoscience and Nanotechnology-Nanocenter, Ljubljana, Slovenia, to access the SEM/EDS scientific equipment.

Appendix A. Supporting information

Supplementary data associated with this article can be found in the online version at doi:10.1016/j.corsci.2024.112551.

Data availability

Data will be made available on request.

References

[1] K. Ogle, R.G. Buchheit, Conversion Coatings, in: A.J. Bard, M. Stratmann (Eds.), Encyclopedia of Electrochemistry, Wiley-VCH, Weinheim, 2003, https://doi.org/10.1002/9783527610426.bard040503.
[2] Regulation (EC) No 1907/2006 of the European Parliament and of the Council of 18 December 2006 concerning the Registration, Evaluation, Authorisation and Restriction of Chemicals (REACH), 2014 (2023).
[3] T.R. Giles, B.H. Goodreau, W.E. Fristad, J. Krömer, P. Droniou, New Generation Conversion Coatings for the Automotive Industry, (2007) 172–181. https://doi.org/10.4271/2007-01-0416.
[4] S. Atkinson, Thin-film conversion coatings reduce process times and costs, Seal. Technol. 2018 (2018) 6, https://doi.org/10.1016/S1350-4789(18)30472-0.
[5] I. Milošev, G. Frankel, Review—Conversion Coatings Based on Zirconium and/or Titanium, J. Electrochem Soc. 165 (2018) C127–C144, https://doi.org/10.1149/2.0371803jes.
[6] W. Revie. Uhlig's Corrosion Handbook, Wiley, Hoboken, NJ, USA, 2011, https://doi.org/10.1002/9780470872864.
[7] W.S. Miller, L. Zhuang, J. Bottema, A.J. Wittebrood, P. De Smet, A. Haszler, A. Vieregge, Recent development in aluminium alloys for the automotive industry, Mater. Sci. Eng.: A 280 (2000) 37–49, https://doi.org/10.1016/S0921-5093(99)00653-X.
[8] A.R. Marder, The metallurgy of zinc-coated steel, Prog. Mater. Sci. 45 (2000) 191–271, https://doi.org/10.1016/S0079-6425(98)00006-1.
[9] A. Nishimoto, J. Inagaki, K. Nakaoka, Effects of surface microstructure and chemical compositions of steels on formation of Fe-Zn compounds during continuous galvanizing, Trans. Iron Steel Inst. Jpn. 26 (1986) 807–813, https://doi.org/10.2355/isijinternational1966.26.807.
[10] M.J. Anderson, P.J. Whitcomb. DOE Simplified, third ed., Productivity Press, New York, 2017 https://doi.org/10.1201/b18479.
[11] M.J. Anderson, P.J. Whitcomb. RSM Simplified, second ed., Productivity Press, New York, 2016 https://doi.org/10.1201/9781315382326.
[12] D. Kramar, Process modelling using design of experiments, in: G. Globočki-Lakić, D. Kramar, J. Kopač (Eds.), Metal Cutting-Theory and Applications, Faculty of Mechanical Engineering, University of Banja Luka and Faculty of Mechanical Engineering, University of Ljubljana, Banja Luka and Ljubljana, 2014.
[13] M. Nabizadeh, K. Marcoen, E. Amine Mernissi Cherigui, M. Dabiri Havigh, T. Kolberg, D. Schatz, H. Terryn, T. Hauffman, Investigation of hybrid Zr-aminosilane treatment formation on zinc substrate and comparison to advanced high strength stainless steel, Appl. Surf. Sci. 610 (2023) 155554, https://doi.org/10.1016/j.apsusc.2022.155554.
[14] G. Šekularac, I. Milošev, Electrochemical behavior and self-sealing ability of zirconium conversion coating applied on aluminum alloy 3005 in 0.5 M NaCl solution, J. Electrochem Soc. 167 (2020) 021509, https://doi.org/10.1149/1945-7111/ab6b0d.
[15] G. Šekularac, J. Kovač, I. Milošev, Comparison of the electrochemical behaviour and self-sealing of zirconium conversion coatings applied on aluminium alloys of series 1xxx to 7xxx, J. Electrochem Soc. 167 (2020) 111506, https://doi.org/10.1149/1945-7111/aba875.
[16] G. Šekularac, J. Kovač, I. Milošev, Prolonged protection, by zirconium conversion coatings, of AlSi7Mg0.3 aluminium alloy in chloride solution, Corros. Sci. 169 (2020) 108615, https://doi.org/10.1016/j.corsci.2020.108615.
[17] M. Mujdrica Kim, B. Kapun, U. Tiringer, G. Šekularac, I. Milošev, Protection of aluminum alloy 3003 in sodium chloride and simulated acid rain solutions by commercial conversion coatings containing Zr and Cr, Coatings 9 (2019) 563, https://doi.org/10.3390/coatings9090563.
[18] S. Adhikari, K.A. Unocic, Y. Zhai, G.S. Frankel, J. Zimmerman, W. Fristad, Hexafluorozirconic acid based surface pretreatments: Characterization and performance assessment, Electrochim. Acta 56 (2011) 1912–1924, https://doi.org/10.1016/j.electacta.2010.07.037.
[19] H. Eivaz Mohammadloo, A.A. Sarabi, Ti-based conversion coatings on cold-rolled steel substrate: the effect of practical parameters and Ti source on surface and

electrochemical properties, CORROSION 72 (2016) 791–804, https://doi.org/10.5006/1936.
[20] A. Kraš, I. Milošev, The aqueous chemistry of zirconium as a basis for better understanding the formation of zirconium conversion coatings: updated thermodynamic data, J. Electrochem Soc. 170 (2023) 21508, https://doi.org/10.1149/1945-7111/acb9c2.
[21] K. Ogle, M. Wolpers, Phosphate Conversion Coatings, in: S.D. Cramer, B.S. Covino (Eds.), Corrosion: Fundamentals, Testing, and Protection, ASM International, 2003, pp. 712–719, https://doi.org/10.31399/asm.hb.v13a.a0003678.
[22] K. Li, J. Liu, T. Lei, T. Xiao, Optimization of process factors for self-healing vanadium-based conversion coating on AZ31 magnesium alloy, Appl. Surf. Sci. 353 (2015) 811–819, https://doi.org/10.1016/j.apsusc.2015.07.052.
[23] P. Santa Coloma, U. Izagirre, Y. Belaustegi, J.B. Jorcin, F.J. Cano, N. Lapeña, Chromium-free conversion coatings based on inorganic salts (Zr/Ti/Mn/Mo) for aluminum alloys used in aircraft applications, Appl. Surf. Sci. 345 (2015) 24–35, https://doi.org/10.1016/j.apsusc.2015.02.179.
[24] S. Wery, M. De Petris-Wery, M. Feki, H.F. Ayedi, Application of a factorial design to study a chromate-conversion process, J. Coat. Technol. Res. 7 (2010) 39–47, https://doi.org/10.1007/s11998-008-9150-4.
[25] P. Puomi, H.M. Fagerholm, J.B. Rosenholm, R. Sipilä, Optimization of commercial zirconic acid based pretreatment on hot-dip galvanized and Galfan coated steel, Surf. Coat. Technol. 115 (1999) 79–86, https://doi.org/10.1016/S0257-8972(99)00171-1.
[26] J. Reck, Y.-M. Wang, H.-H.H. Kuo, Development of Zirconium-based Conversion Coatings for the Pretreatment of AZ91D Magnesium Alloy Prior to Electrocoating. in: Magnesium Technology, Springer International Publishing, Cham, 2011, pp. 523–529, https://doi.org/10.1007/978-3-319-48223-1_97.
[27] Y. Huang, F. Mansfeld, Evaluation of the effects of different process parameters on the corrosion protection provided by cerium-based coatings on galvanized steels, CORROSION 65 (2009) 507–510, https://doi.org/10.5006/1.3319154.
[28] S. El Hajjaji, A. Lgamri, E. Puech-Costes, A. Guenbour, A. Ben Bachir, L. Aries, Optimization of conversion coatings: study of the influence of parameters with experimental designs, Appl. Surf. Sci. 165 (2000) 184–192, https://doi.org/10.1016/S0169-4332(00)00444-X.
[29] ASTM International, ASTM G31-72(2004), Standard Practice for Laboratory Immersion Corrosion Testing of Metals, (2012), https://doi.org/10.1520/G0031-72R04.
[30] G.S. Frankel, M. Rohwerder, Electrochemical Techniques for Corrosion, in: M. Stratmann, G.S. Frankel (Eds.), Encyclopedia of Electrochemistry, Wiley, Weinheim, 2003, https://doi.org/10.1002/9783527610426.bard040007.
[31] D. Ho, N. Brack, J. Scully, T. Markley, M. Forsyth, B. Hinton, Cerium dibutylphosphate as a corrosion inhibitor for AA2024-T3 aluminum alloys, J. Electrochem Soc. 153 (2006) B392, https://doi.org/10.1149/1.2217260.
[32] P. Rodič, I. Milošev, G.S. Frankel, Corrosion of synthetic intermetallic compounds and AA7075-T6 in dilute Harrison's solution and inhibition by cerium(III) salts, J. Electrochem Soc. 170 (2023) 031503, https://doi.org/10.1149/1945-7111/acc0a3.
[33] F.D. Timmins, Avoiding paint failures by prohesion, J. Oil. Col. Chem. Assoc. 62 (1979) 131–135.
[34] J.B. Harrison, T.C.K. Tickle, New aspects of the atmospheric corrosion of steel and their implications, J. Oil Colour. Chem. ' Assoc. 45 (1962) 571–597.
[35] R.L. Howard, S.B. Lyon, J.D. Scantlebury, Accelerated tests for the prediction of cut-edge corrosion of coil-coated architectural cladding, Prog. Org. Coat. 37 (1999) 91–98, https://doi.org/10.1016/S0300-9440(99)00060-0.
[36] J.B. Harrison, Prediction of performance of primers and its relationship to the performance of a full paint system in practice, Br. Corros. J. 4 (1969) 58–65, https://doi.org/10.1179/000705969798325596.
[37] G. Gusmano, G. Montesperelli, M. Rapone, G. Padeletti, A. Cusmà, S. Kaciulis, A. Mezzi, R.Di Maggio, Zirconia primers for corrosion resistant coatings, Surf. Coat. Technol. 201 (2007) 5822–5828, https://doi.org/10.1016/J.SURFCOAT.2006.10.036.
[38] S. Wang, J. Zhang, O. Gharbi, V. Vivier, M. Gao, M.E. Orazem, Electrochemical impedance spectroscopy, Nat. Rev. Methods Prim. 1 (2021) 41, https://doi.org/10.1038/s43586-021-00039-w.
[39] F.L. Floyd, S. Avudaiappan, J. Gibson, B. Mehta, P. Smith, T. Provder, J. Escarsega, Using electrochemical impedance spectroscopy to predict the corrosion resistance of unexposed coated metal panels, Prog. Org. Coat. 66 (2009) 8–34, https://doi.org/10.1016/j.porgcoat.2009.04.009.
[40] F.L. Floyd, S. Tatti, T. Provder, Using DC electrochemical techniques to assess the relative corrosiveness of water-based coatings and their ingredients, J. Coat. Technol. Res 4 (2007) 111–129, https://doi.org/10.1007/s11998-007-9012-5.
[41] R. Srinivasan, F. Fasmin. An Introduction to Electrochemical Impedance Spectroscopy, 1st ed., CRC Press, Boca Raton, 2021 https://doi.org/10.1201/9781003127932.
[42] ГОСТ 9.302-88. Edinaya sistema zashchity ot korrozii i stareniya. Pokrytiya metallicheskie i nemetallicheskie neorganicheskie, Metodykontrolya, Izd. Standardov, Moscow, 1990.
[43] A. Cox, S.B. Lyon, An electrochemical study of the atmospheric corrosion of mild steel-I. Experimental method, Corros. Sci. 36 (1994) 1167–1176, https://doi.org/10.1016/0010-938X(94)90141-4.
[44] F. Mansfeld, Electrochemical impedance spectroscopy (EIS) as a new tool for investigating methods of corrosion protection, Electrochim. Acta 35 (1990) 1533–1544, https://doi.org/10.1016/0013-4686(90)80007-B.
[45] A. Kraš, I. Milošev, Comparative electrochemical and thermodynamic study of cold-rolled steel, Al alloy AA5754, and Zn corrosion in fluoride and chloride solutions, Electrochim. Acta 502 (2024) 144819, https://doi.org/10.1016/j.electacta.2024.144819.
[46] D. Chidambaram, C.R. Clayton, G.P. Halada, The role of hexafluorozirconate in the formation of chromate conversion coatings on aluminum alloys, Electrochim. Acta 51 (2006) 2862–2871, https://doi.org/10.1016/j.electacta.2005.08.022.
[47] ASTM International, ASTM F22-21, Standard Test Method for Hydrophobic Surface Films by the Water-Break Test, (2021), https://doi.org/10.1520/F0022-21.
[48] S. Mancini, Conversion Coatings: Phosphate vs. Zirconium | Products Finishing, (2018), https://www.pfonline.com/articles/conversion-coatings-phosphate-vs-zirconium- (accessed October 18, 2023).
[49] A. Clearfield, G.P.D. Serrette, A.H. Khazi-Syed, Nature of hydrous zirconia and sulfated hydrous zirconia, Catal. Today 20 (1994) 295–312, https://doi.org/10.1016/0920-5861(94)80008-1.
[50] A. Clearfield, The mechanism of hydrolytic polymerization of zirconyl solutions, J. Mater. Res 5 (1990) 161–162, https://doi.org/10.1557/JMR.1990.0161.
[51] C.E. Tomlinson, Chromate-free conversion coatings for metals, US5759244A, 1998. ⟨https://patents.google.com/patent/US5759244A/en⟩ (accessed March 25, 2024).
[52] R.G. Kelly, J.R. Scully, D. Shoesmith, R.G. Buchheit, Electrochemical Techniques in Corrosion Science and Engineering, CRC Press, 2002, https://doi.org/10.1201/9780203909133.
[53] ASTM International, ASTM G59-97(2020), Standard Test Method for Conducting Potentiodynamic Polarization Resistance Measurements, (2023). https://doi.org/10.1520/G0059-97R20.
[54] L. Wang, D. Snihirova, M. Deng, C. Wang, B. Vaghefinazari, G. Wiese, M. Langridge, D. Höche, S.V. Lamaka, M.L. Zheludkevich, Insight into physical interpretation of high frequency time constant in electrochemical impedance spectra of Mg, Corros. Sci. 187 (2021) 109501, https://doi.org/10.1016/j.corsci.2021.109501.
[55] I. Thompson, D. Campbell, Interpreting Nyquist responses from defective coatings on steel substrates, Corros. Sci. 36 (1994) 187–198, https://doi.org/10.1016/0010-938X(94)90119-8.
[56] M.E. Orazem, B. Tribollet, Electrochemical Impedance Spectroscopy, Wiley, 2008, https://doi.org/10.1002/9780470381588.
[57] D.H. van der Weijde, E.P.M. van Westing, J.H.W. de Wit, Electrochemical techniques for delamination studies, Corros. Sci. 36 (1994) 643–652, https://doi.org/10.1016/0010-938X(94)90070-1.
[58] E. Barsoukov, J.R. Macdonald, Impedance Spectroscopy, Wiley, 2005, https://doi.org/10.1002/0471716243.
[59] C.C. Herrmann, G.G. Perrault, A.A. Pilla, Dual reference electrode for electrochemical pulse studies, Anal. Chem. 40 (1968) 1173–1174, https://doi.org/10.1021/ac60263a011.
[60] F. Mansfeld, S. Lin, Y.C. Chen, H. Shih, Minimization of high-frequency phase shifts in impedance measurements, J. Electrochem Soc. 135 (1988) 906–907, https://doi.org/10.1149/1.2095825.
[61] H.R.P. Cardoso, C. Rapacki, J.Z. Ferreira, Monitoring of a Zr-based conversion coating on galvanised steel and its performance against corrosion, Corros. Eng. Sci. Technol. 54 (2019) 726–730, https://doi.org/10.1080/1478422X.2019.1657703.
[62] J.A. Grandle, S.R. Taylor, Electrochemical impedance spectroscopy of coated aluminum beverage containers: part 1 — determination of an optimal parameter for large sample evaluation, CORROSION 50 (1994) 792–803, https://doi.org/10.5006/1.3293469.
[63] A. Ghanbari, M.M. Attar, Corrosion behavior of zirconium treated mild steel with and without organic coating: a comparative study, Surf. Rev. Lett. 21 (2014) 1450088, https://doi.org/10.1142/S0218625X14500887.
[64] A. Lasia, Electrochemical Impedance Spectroscopy and its Applications, Springer New York, New York, NY, 2014, https://doi.org/10.1007/978-1-4614-8933-7.
[65] A. Niaz, Complementary use of electrochemical testing techniques to study corrosion processes of HVOF Inconel 625. CoNiCrAlY and WCCoCr coatings, University of Nottingham, 2013. PhD thesis.
[66] P. Campestrini, E.P.M. van Westing, J.H.W. de Wit, Influence of surface preparation on performance of chromate conversion coatings on Alclad 2024 aluminium alloy: part II: EIS investigation, Electrochim. Acta 46 (2001) 2631–2647, https://doi.org/10.1016/S0013-4686(01)00476-5.
[67] H. Otmacic Curkovic, E. Stupnisek-Lisac, H. Takenouti, Electrochemical quartz crystal microbalance and electrochemical impedance spectroscopy study of copper corrosion inhibition by imidazoles, Corros. Sci. 51 (2009) 2342–2348, https://doi.org/10.1016/j.corsci.2009.06.018.
[68] C.M. Abreu, M.J. Cristóbal, R. Losada, X.R. Nóvoa, G. Pena, M.C. Pérez, High frequency impedance spectroscopy study of passive films formed on AISI 316 stainless steel in alkaline medium, J. Electroanal. Chem. 572 (2004) 335–345, https://doi.org/10.1016/j.jelechem.2004.01.015.
[69] C. Andrade, M. Keddam, X.R. Nóvoa, M.C. Pérez, C.M. Rangel, H. Takenouti, Electrochemical behaviour of steel rebars in concrete: influence of environmental factors and cement chemistry, Electrochim. Acta 46 (2001) 3905–3912, https://doi.org/10.1016/S0013-4686(01)00678-8.
[70] M. Özcan, İ. Dehri, M. Erbil, EIS study of the effect of high levels of SO_2 on the corrosion of polyester-coated galvanised steel at different relative humidities, Prog. Org. Coat. 44 (2002) 279–285, https://doi.org/10.1016/S0300-9440(02)00060-7.
[71] Q. Jiang, Q. Miao, F. Tong, Y. Xu, B. Ren, Z. Liu, Z. Yao, Electrochemical corrosion behavior of arc sprayed Al–Zn–Si–RE coatings on mild steel in 3.5% NaCl solution, Trans. Nonferrous Met. Soc. China 24 (2014) 2713–2722, https://doi.org/10.1016/S1003-6326(14)63402-6.

[72] A. Collazo, X.R. Nóvoa, C. Pérez, B. Puga, EIS study of the rust converter effectiveness under different conditions, Electrochim. Acta 53 (2008) 7565–7574, https://doi.org/10.1016/j.electacta.2007.11.078.
[73] N.B. Pilling, R.E. Bedworth, The oxidation of metals at high temperature, J. Inst. Met. 29 (1923) 529–582.
[74] J.R. Scully, Polarization resistance method for determination of instantaneous corrosion rates, CORROSION 56 (2000) 199–218, https://doi.org/10.5006/1.3280536.
[75] I. Frateur, C. Deslouis, M.E. Orazem, B. Tribollet, Modeling of the cast iron/drinking water system by electrochemical impedance spectroscopy, Electrochim. Acta 44 (1999) 4345–4356, https://doi.org/10.1016/S0013-4686(99)00150-4.
[76] A. Lasia, Impedance of porous electrodes, J. Electroanal. Chem. 397 (1995) 27–33, https://doi.org/10.1016/0022-0728(95)04177-5.
[77] R. de Levie, On porous electrodes in electrolyte solutions, Electrochim. Acta 8 (1963) 751–780, https://doi.org/10.1016/0013-4686(63)80042-0.
[78] J.M. Hu, J.Q. Zhang, C.N. Cao, Determination of water uptake and diffusion of Cl− ion in epoxy primer on aluminum alloys in NaCl solution by electrochemical impedance spectroscopy, Prog. Org. Coat. 46 (2003) 273–279, https://doi.org/10.1016/S0300-9440(03)00010-9.
[79] I. Milošev, T.K. Mikić, M. Gaberšček, The effect of Cu-rich sub-layer on the increased corrosion resistance of Cu–xZn alloys in chloride containing borate buffer, Electrochim. Acta 52 (2006) 415–426, https://doi.org/10.1016/j.electacta.2006.05.024.
[80] T. Kosec, D.K. Merl, I. Milošev, Impedance and XPS study of benzotriazole films formed on copper, copper–zinc alloys and zinc in chloride solution, Corros. Sci. 50 (2008) 1987–1997, https://doi.org/10.1016/j.corsci.2008.04.016.
[81] C. Montella, Voigt circuit representation model for electrochemical impedances under finite-length diffusion conditions, J. Electroanal. Chem. 879 (2020) 114785, https://doi.org/10.1016/j.jelechem.2020.114785.
[82] P. Leuaa, D. Priyadarshani, A.K. Tripathi, M. Neergat, Internal and external transport of redox species across the porous thin-film electrode/electrolyte interface, J. Phys. Chem. C. 123 (2019) 21440–21447, https://doi.org/10.1021/acs.jpcc.9b02795.
[83] M. Schönleber, E. Ivers-Tiffée, Approximability of impedance spectra by RC elements and implications for impedance analysis, Electrochem. Commun. 58 (2015) 15–19, https://doi.org/10.1016/j.elecom.2015.05.018.
[84] P. Agarwal, M.E. Orazem, L.H. Garcia-Rubio, Measurement models for electrochemical impedance spectroscopy: I. demonstration of applicability, J. Electrochem Soc. 139 (1992) 1917–1927, https://doi.org/10.1149/1.2069522.
[85] Y.-K. Song, F. Mansfeld, Evaluation of the corrosion resistance of different galvanized steels treated in a cerium salt solution, Mater. Corros. 56 (2005) 229–236, https://doi.org/10.1002/maco.200403830.
[86] G.S. Frankel, in: A.E. Hughes, J.M.C. Mol, M.L. Zheludkevich, R.G. Buchheit (Eds.), Fundamentals of Corrosion Kinetics, Springer Netherlands, Dordrecht, 2016, pp. 17–32, https://doi.org/10.1007/978-94-017-7540-3_2.
[87] G.E.P. Box, W.G. Hunter, S.J. Hunter, Statistics for Experimenters: Design, Innovation, and Discovery, Wiley, New York, 2005.
[88] R. Yang, P.Y. Xu, Y. Jing, G. Xin, Evaluating the anti-corrosion behavior of hybrid zirconium-polyethyleneimine layer by mean of electrochemical method, J. Phys. Conf. Ser. 1605 (2020) 012159, https://doi.org/10.1088/1742-6596/1605/1/012159.
[89] J. Konopka, Examination of the Fluorine K Line and Iron L Line Overlap by EDS and WDS, Application Note 52455, Madison, WI, USA, 2013. ⟨www.thermoscientific.com⟩.
[90] J.I. Goldstein, D.E. Newbury, J.R. Michael, N.W.M. Ritchie, J.H.J. Scott, D.C. Joy, Scanning Electron Microscopy and X-Ray Microanalysis, Springer New York, New York, NY, 2018, https://doi.org/10.1007/978-1-4939-6676-9.
[91] R.K. Mishra, A.K. Zachariah, S. Thomas, Energy-Dispersive X-ray Spectroscopy Techniques for Nanomaterial. in: Microscopy Methods in Nanomaterials Characterization, Elsevier, 2017, pp. 383–405, https://doi.org/10.1016/B978-0-323-46141-2.00012-2.
[92] M. Pourbaix. Atlas of Electrochemical Equilibria in Aqueous Solutions, 2nd ed., National Association of Corrosion Engineers, Texas, 1974.
[93] Y. Zhai, Z. Zhao, G.S. Frankel, J. Zimmerman, T. Bryden, W. Fristad, A Replacement for Phosphate Conversion Coating Based on Hexafluorozirconic Acid, SAE Technical Paper 2008-01-1158, 2008, https://doi.org/10.4271/2008-01-1158.
[94] A. Kraš, I. Milošev, A. Seyeux, P. Marcus, Polymerised forms in the zirconium conversion coatings on cold-rolled steel: proof of concept, Npj Mater. Degrad. 8 (2024) 65, https://doi.org/10.1038/s41529-024-00485-3.
[95] T. Lostak, S. Krebs, A. Maljusch, T. Gothe, M. Giza, M. Kimpel, J. Flock, S. Schulz, Formation and characterization of Fe^{3+}-/Cu^{2+}-modified zirconium oxide conversion layers on zinc alloy coated steel sheets, Electrochim. Acta 112 (2013) 14–23, https://doi.org/10.1016/j.electacta.2013.08.161.
[96] H. Eivaz Mohammadloo, A.A. Sarabi, A.A. Sabbagh Alvani, H. Sameie, R. Salimi, Nano-ceramic hexafluorozirconic acid based conversion thin film: surface characterization and electrochemical study, Surf. Coat. Technol. 206 (2012) 4132–4139, https://doi.org/10.1016/j.surfcoat.2012.04.009.
[97] B. Szczygieł, J. Winiarski, W. Tylus, Effect of deposition time on morphology, corrosion resistance and mechanical properties of Ti-containing conversion coatings on zinc, Mater. Chem. Phys. 129 (2011) 1126–1131, https://doi.org/10.1016/j.matchemphys.2011.05.074.
[98] A. Yi, J. Du, J. Wang, S. Mu, G. Zhang, W. Li, Preparation and characterization of colored Ti/Zr conversion coating on AZ91D magnesium alloy, Surf. Coat. Technol. 276 (2015) 239–247, https://doi.org/10.1016/j.surfcoat.2015.06.069.
[99] X. Chen, G. Li, J. Lian, Q. Jiang, Study of the formation and growth of tannic acid based conversion coating on AZ91D magnesium alloy, Surf. Coat. Technol. 204 (2009) 736–747, https://doi.org/10.1016/j.surfcoat.2009.09.022.
[100] N.W. Khun, G.S. Frankel, Effect of hexafluorozirconic acid pretreatment on cathodic delamination of epoxy coatings from steel substrates, CORROSION 71 (2015) 277–284, https://doi.org/10.5006/1407.
[101] H. Eivaz Mohammadloo, A.A. Sarabi, R. Mohammad Hosseini, M. Sarayloo, H. Sameie, R. Salimi, A comprehensive study of the green hexafluorozirconic acid-based conversion coating, Prog. Org. Coat. 77 (2014) 322–330, https://doi.org/10.1016/j.porgcoat.2013.10.006.
[102] P. Cao, X. Zhou, L. Ran, J. Tang, J. Yang, The 3D nano-trench interface to manipulate the stripping/plating behavior for stable Zn anode, J. Power Sources 528 (2022) 231215, https://doi.org/10.1016/j.jpowsour.2022.231215.
[103] S. Thomas, N. Birbilis, M.S. Venkatraman, I.S. Cole, Corrosion of zinc as a function of pH, CORROSION 68 (2012) 015009-1–015009-9, https://doi.org/10.5006/1.3676630.
[104] C.G. da Silva, I.C.P. Margarit-Mattos, O.R. Mattos, H. Perrot, B. Tribollet, V. Vivier, The molybdate-zinc conversion process, Corros. Sci. 51 (2009) 151–158, https://doi.org/10.1016/j.corsci.2008.10.019.